NUMERICAL INVESTIGATION OF Y-SHAPED AND CSC MICROMIXERS

A Thesis Submitted to
the Graduate School of Engineering and Sciences of
İzmir Institute of Technology
in Partial Fulfilment of the Requirements for the Degree of

MASTER OF SCIENCE

in Mechanical Engineering

by
Umut Ege SAMANCIOĞLU

December 2022
İZMİR

ACKNOWLEDGMENTS

At first, I would like to thank to my supervisor, Prof. Dr. Erdal ÇETKİN for his guidance, imparted wisdom, and patience through my theses.

I would like to thank to Resul Çağtay ŞAHİN to help me find the key for my validation study, my laboratory partners for creating an enjoyable working environment and my family to believing in me and offering me a calming safe zone and understanding me in my stressful days.

ABSTRACT

NUMERICAL INVESTIGATION OF Y-SHAPED AND CSC MICROMIXERS

Micromixers are one of the key parts in microfluidic devices. Therefore, passive micromixers have become a popular research topic. In this thesis, parametric optimization of a Y-shaped micromixer with mixing chamber is documented. Design parameters are; alpha (α) for the angle between the two inlet angles, beta (β) for the angle between the z axis and one of the inlet channels and theta (θ) for the angle between the other inlet channel, z-eccentricity (z_{ecc}) is the distance between the centerline of an inlet channel and origin of the mixing chamber along z-axis, x-eccentricity (x_{ecc}) is the distance between the intersection point of the two inlets and the origin of the mixing chamber along x-axis, ratio of the inlet and outlet channel length (L_1/L_2), ratio of the inlet and outlet channel diameter (D_1/D_2), ratio of the inlet channel length and diameter (L_2/D_2) and ratio of mixing chamber volume to the total volume(V_{sp}). α= 180^o - 240^o range and z_{ecc}= 20μm corresponds to the optimal range. Effect of each parameter on the system is discussed and the best performing 3 mixer designs are further investigated. The optimized design yields 88.16% mixing efficiency with 9244.4 Pa pressure drop when Reynolds number is 81. Furthermore, performance of this design is compared with a reference design. The comparison shows that optimized design decreases the pressure drop more than 50% for all Reynolds numbers while having a higher mixing efficiency (up to 35%) with low Reynolds numbers (0.054-3).

Keywords: Passive Micromixer, 3-D Micromixer, Mixing Chamber, Y-Shaped Micromixer

ÖZET

Y-ŞEKİLLİ VE CSC MİKROKARIŞTIRICILARIN SAYISAL İNCELENMESİ

Verimlilik üzerine artan odak nedeniyle mikroakış cihazları üzerindeki ilgi artmaktadır. Mikrokarıştırıcılar mikroakış cihazlarının anahtar parçalarından biridir. Bu nedenle pasif mikrokarıştırıcılar popüler bir araştırma konusu haline gelmiştir. Bu tezde Y-şekilli ve karıştırma hazneli mikrokarıştırıcı üzerinde parametrik bir çalışma anlatılmaktadır. Bu mikrokarıştırıcı için tasarım parametreleri; iki giriş kanalı arasındaki açı alfa (α), z ekseni ile giriş kanallarından biri arasındaki açı beta (β) ve diğer giriş kanalı ile z ekseni arasındaki açı teta (θ), giriş kanalı merkez çizgisi ile karıştırma küresinin merkez noktası arasındaki z ekseni üzerindeki mesafe z-eksantrikliği (z_{ecc}), iki giriş kanalının kesişim noktası ile karıştırma küresinin merkez noktası arasındaki x ekseni üzerindeki mesafe x- eksantrikliği (x_{ecc}), giriş ve çıkış kanallarının uzunluklarının oranı (L_1/L_2), giriş ve çıkış kanallarının çaplarının oranı (D_1/D_2), giriş kanalının uzunluğunun çapına oranı (L_2/D_2) ve karıştırma küresi hacminin toplam hacme oranı (V_{sp}). α açısının 180^o - 240^o aralığında ve z_{ecc}'nin 20μm değerinde optimum olarak değerlendirilebileceği görüldü. Ancak β açıları için ya da x_{ecc} için spesifik bir değer bulunamadı. Tüm tasarım parametrelerinin sisteme olan etkisi tartışıldı ve en iyi karıştırma verimine sahip 3 tasarım incelenmeye devam edildi. Sonuç olarak 1. tasarımın optimum tasarım için iyi bir yakınsama olacağı düşünüldü. Seçilen tasarım Reynolds sayısı 81 iken %88.16 karıştırma verimini 9244.4 Pa basınç düşümü ile verebilmektedir. Sonrasında bu tasarımın performansı çalışmanın sağlaması için kullanılan temel tasarımın performansı ile karşılaştırıldı. Bu karşılaştırma ile seçilen tasarımın temel tasarıma göre tüm Reynolds sayılarında %50 basınç düşümü tasarrufu yaptığı ve düşük Reynolds sayılarında (0.054-3) %35'e kadar daha yüksek karıştırma verimi elde ettiği görüldü.

Anahtar Kelimeler: Pasif Mikrokarıştırıcı, 3-B Mikrokarıştırıcı, Karıştırma Hazneli Mikrokarıştırıcı, Y-Şekilli Mikrokarıştırıcı

TABLE OF CONTENTS

LIST OF FIGURES

Figure **Page**

Figure **Page**

LIST OF TABLES

Table **Page**

LIST OF SYMBOLS

Nomenclature

A	surface area [m^2]
c	concentration
$\bar{c}$	average concentration
D	duct diameter [m]
D_c	diffusion coefficient [$m^2\ s^{-1}$]
d_h	hydraulic diameter [m]
L	duct length [m]
M	mixing efficiency
P	pressure [Pa]
Re	Reynolds number
u	velocity [$m\ s^{-1}$]
$\bar{u}$	mean outlet channel velocity [$m\ s^{-1}$]
x,y,z	directions

Greek letters

α, β, θ	angles
σ	mole concentration fraction standard deviation
σ_0	average mole concentration fraction standard deviation
ϑ	kinematic viscosity [$m^2\ s^{-1}$]
μ	viscosity [Pa s]
ρ	density [$kg\ m^{-3}$]

Subscripts

1	outlet duct
2	inlet duct
i	index
sp	sphere

CHAPTER 1

INTRODUCTION

1.1. Microfluidic Devices

With the miniaturization trend, interest over the microelectromechanical systems (MEMS) and microfluidic devices enhanced [1] [2]. Lab-on-chip applications, micro total analysis systems and micro reactors can be listed as some examples of the microfluidic devices [2] [3]. Microfluidic chip can be described as a network of microchannels that is connected to the microenvironment via several holes through the device. In figure 1.1 connections and a lab-on-chip device is presented. Lab-on-chip applications achieves to integrate biological and chemical processes on a single micro device. These devices are being used in polymetric particle synthesis such as drug delivery vehicles or bioarchitecture models like liver-on-chip or cancer cell mimicking devices. Polymers or glass can be used for manufacturing these devices; however, polymers are widely preferred in the industry because of their cost efficiency, suitable optical transparency, elasticity and preferrable chemical and mechanical properties [4] [5].

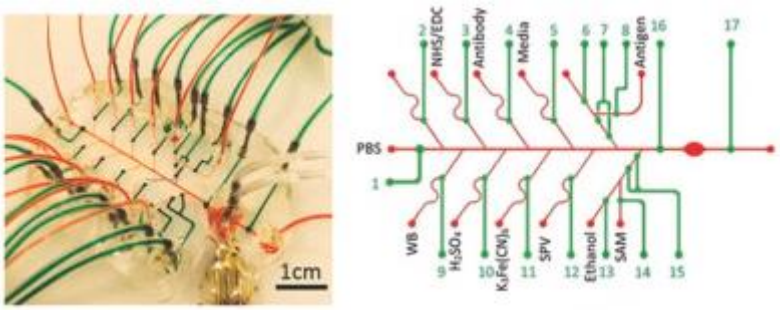

Figure 1.1. Liver-on-chip application [5]

Even though micro reactors were first introduced in early 90's to the field, recently they find increasing use on various fields such as; chemical industry, biological industry, pharmaceutical industry, clinical diagnosis etc. Furthermore, they are applied in fields such as; nanomaterial synthesis, clinical diagnostics, medical monitoring, quality control, etc. [3 6]. Song et al. [3] in their review mentioned that by using lab-on-a-chip systems in synthesis of nanoparticles, advantages like superior control over the shape, size and structure of nanoparticles, ability to adjust nucleation growth rate can be benefitted. They suggested that an increase in monodispercity by just downsizing from bulk production to microliter volume can be seen. Also, microreactors are able to mass produce using continuous flow processes and parallel connections of microreactors. Further increase in monodispercity can be attained with efficient mixing inside the microreactor, therefore most microreactors used in nanoparticle synthesis processes possess micromixers, microchannels and microheaters [3]. Chen et al. [7] designed a microchip based on localized surface plasmon resonance (LSPR) to detect multiple cytokine biomarkers. Cytokines are critically important in monitoring the health status of the patient and enables doctors to create and adjust treatment strategies for diseases like cancer, lupus, sepsis and graft-versus-host disease. Because of the importance of quantifying cytokines in a human serum, real time or near real time monitoring would be beneficial. The designed chip successfully quantified six different cytokine biomarkers related with organ failure and bacterial infections with miniature serum samples. Also, they succeeded to quantify cytokine biomarkers in less than 30 minutes with this microchip instead of 8 hours that would normally take with conventional methods [7]. Glawdel et al. [8] produced a portable microfluidic system to test the toxicity of water. The device involves an electroosmotic pump, concentration gradient generator and fish cell line. System analyses the toxic chemicals attached to the fish cells to measure the level of toxicity of the water [8]. Minghao et al. [9] designed a fully automated enzyme-linked immuno-sorbent assay (ELISA) system produced on a portable disc to test blood for infectious diseases. The device is shown in figure 1.2. In the figure three layered structure of the device is shown. Where the first layer has the purpose of extracting the serum, in second layer diluent distribution is made and in the third layer contains the preloaded liquid storage chamber, reaction chamber and detection chamber where magnetic beads coated with capture antibody are used with enzyme coated with detection antibody. The product tested for the antigen and the antibody of Hepatitis B virus (HBV), HBsAg and Anti-HBs. System was preloaded with all the necessary

reagents and was able to complete the test in 30 mins opposed to 2 hours that would take normally with having the same detection limit [9].

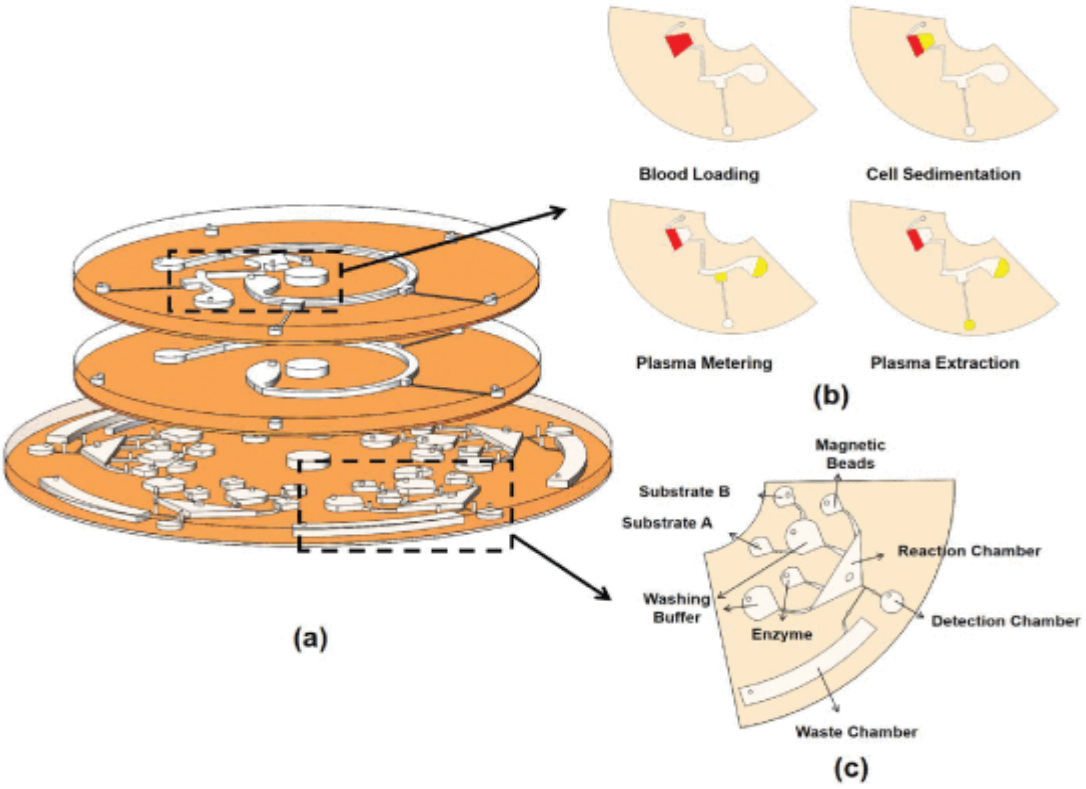

Figure 1.2. ELISA portable disc [9]

Suarez et al. [10] constructed a lab on a chip immunoassay-based antibiotic sensing device to detect antibiotics in raw milk. The chip involved a polymer based microfluidic cartridge and wavelength interrogated optical sensor. Device successfully identified three antibiotic families with 95% accuracy in less than 10 minutes [10]. Walsh et al. [11] produced a microfluidic device to mimic tumors by recreating microenvironment gradients of a tumor in order to uncover the heterogeneity of the microenvironment which limits the effectiveness of the cancer treatment. They used a polydimethylsiloxane (PDMS) and glass device and presented that the cell mass contained was demonstrative of a vivo tumor. They accurately measured diffusion coefficient of doxorubicin and therapeutic bacteria accumulation with the use of fluorescence microscopy. They suggested that their device is going to be crucial in

understanding cancer drug behavior inside solid tumors [11]. As it can be seen from the wide variety of application examples for microfluidic devices, focus on the microfluidic devices is increasing in various industries and their potential for speed and efficiency regarding both material and time save is being discovered.

1.2. Advantages of Microfluidic Devices

The growth in use of microfluidic devices can be explained by their advantages over the conventional systems. Microfluidic attain more control over the processes by their responsiveness to changing inlet conditions, with the use of their small volume. They allow to keep a smaller inventory, with their ability to fast and accurate production on demand [3 2]. The reduced need for inventory provides risks related with storage of chemicals such as, explosion, leakage of toxic products or risk of passing best before dates to be lessened. Microfluidic devices have the ability to very accurately tweak the reaction parameters such as reagent concentration, temperature and flow rates, combined with the possibility to change or stop the process when the desired amount of product is produced with a sensitivity of up to nanoliter volume, increases the control over the final product greatly compared to conventional batch production [3 12]. It is possible to connect thousands of microfluidic reactors to produce final products with the nanoliter accuracy in large quantities [3 13]. Microfluidic reactors have high surface to volume ratio, offering high heat dissipation rates which creates more active sites. Using micromixers inside microreactors can mix reagents on a short time scale and achieve homogenous flow through the system. Microreactors operate under continuous flow regime which gives the ability to add reagents downstream for multistep reactions, combined with the capability to control the reactions by controlling flow parameters results in having more flexibility in kinetic control of reactions [3].

1.3. Micromixers

Micromixers are critically important for microfluidic devices. These devices require homogenous continuous flow for controllable, fast and accurate reactions. By the virtue of the microscale dimensions of microfluidic systems, flows inside the microchannels are inherently laminar. Absence of turbulence in laminar flow causes the dominant mixing method to be diffusion for these applications. Mixing with diffusion is a tedious process that requires long residence times and long channels in order to provide the necessary residency time. This results in excess use of reagents, higher pressure drop and decrease in system responsiveness [3 7 14 15]. Diffusion rate expression is given, in equation 1 to understand the mixing mechanism of micromixers [2].

$$D_c A \frac{dc}{dx} \quad (1)$$

Where D_c is the diffusion coefficient, A is the mass transfer area and dc/dx is the concentration gradient. Since the diffusion coefficient is dependent on the reagent and it is not a trivial task to adjust the concentration gradient, literature mainly focuses on designs that enhance the mass transfer area between the different concentrations of fluid [2]. Micromixers are generally divided in two groups, active and passive micromixers.

1.3.1. Active Micromixers

Active micromixers require external energy sources to disturb the symmetry of laminar flow and enhance the mass transfer surface area. These external energy sources used in these micromixers can be listed as; acoustic, magnetic, dielectrophoretic, heat etc. [16] Luong et al. [17] produced a surface acoustic wave micromixer. They used water and fluorescent die for visualization. While the fluids are pumped through the syringe pump, surfacewave was generated and launched perpendicularly to the flow with two interdigitized electrodes working at 13 MHz frequency. Their results suggested that mixing efficiency is proportional to the square of the applied voltage and focusing type achieved better mixing with equal voltages. Their proposed micromixer reached an 88%

mixing efficiency [17]. Jeon et al. [18] studied the optimum configuration of electrodes for magnetohydrodynamic mixing. The parameters: shape, configuration, voltage and the micromixer height investigated. After the investigation of six different configurations of electrodes, the best resulting configuration is further studied for micromixer height and applied voltage. They showed that a mixing efficiency of 90% can be achieved with their design and numerical methods are suitable for investigation of optimal configuration for electrodes [18]. Zhang et al. [19] fabricated a micromixer that use induced charge electroosmosis. They used asymmetrical planar floating electrodes to generate asymmetric microvortices inside the flow. Their design achieved a 94.7% mixing efficiency with 400Hz frequency sinusoidal wave with 14V applied voltage [19]. Kunti et al. [20] studied an alternating current electrothermal micromixer. They microgrooved the channel floor and placed asymmetric electrode pairs. Also, an array of symmetric electrodes was introduced to the channel top wall. When operational the asymmetric electrodes induced the fluid flow and the symmetric electrodes generated lateral vortex pairs. Combined with the waviness of the channel resulting from the microgooving, the micromixer act as a semi active semi passive micromixer and achieved a 97.25% mixing efficiency [20]. Even though the active micromixers generally offer higher mixing efficiencies and superior control over the mixing, their need for external energy sources results in complex designs, moving parts, cabling and larger space requirements. Complexity of active micromixers let passive micromixers the preferred choice for the microfluidic applications with their simplicity and compact nature [21].

1.3.2. Passive Micromixers

Passive micromixers do not require an external energy source but use the energy of the flow. Hence, they do not require any additional parts or cabling. Having these advantages, passive micromixers are the preferred option in microfluidic applications. In passive micromixers, the symmetry of the laminar flow is aimed to be broken so that the total mass transfer area increases, or the diffusion length decreases. The flow symmetry is disturbed by either adjusting the outlet channel geometry by adding baffles or ridges to the outlet channel or setting the inlet channels so that they induce chaotic

advection by creating vortex like flow inside the outlet channel [22]. The two main mixing mechanisms that the passive micromixers benefit from are lamination and chaotic advection. In lamination the mixing efficiency is enhanced by either squeezing the flow inside the channel to reduce the overall diffusion length or by dividing the flow by separating it into several channels and combining them later along the mixer to achieve a lamellae with alternating different concentration fluids, so that the total mass transfer area enlarges [2] [15]. On the other hand, the chaotic advection mechanism can be introduced to the system by inserting obstacles inside the outlet channel such as baffles, ridges or gaps or by having design modifications on the inlet channels. In chaotic advection, vortex like structures added inside the flow that generate transverse motion by breaking, folding and stretching the flow. This motion breaks the flow into thin layers which creates a laminated structure of alternating different concentration fluid layers that improves of total mass transfer area [2] [22]. Additional to these mechanisms Dean flow is also used in passive micromixers to induce transverse motion. Dean flow is originated from the interaction of centrifugal and inertial forces with viscous forces while a fluid flows through a curved channel. In micromixers due to low Reynolds numbers usually two counter rotating vortices are generated in Dean flow which creates a transverse motion [23].

Passive micromixer example that uses lamination mechanism with separation of channels method and Dean flow can be given by Sudarsan and Ugaz [23]. They designed a split and recombine micromixer that benefits the Dean flow effect and expansion vortices. They utilized curved channels to induce Dean flow. With the help of the Dean flow vertically laminated flow inside the channel becomes horizontally laminated at point (II) in figure 1.3a. Once the flow is horizontally laminated due to Dean vortices, they separated the flow into several channels. Further curvature of the channels created vertically laminated structure. When the vertical laminated structure constructed the separated channels are combined down in the micromixer, to connect individual vertically laminated structure. In the end the diffusion distance between the two different concentration fluids is greatly decreased. The process repeated along the micromixer until the desired mixing efficiency achieved. Their mixer is presented in figure 1.3. They reported 90% mixing efficiency at k = 9.1. Here k is the Dean Number and represents the relative magnitude of the centrifugal and inertial forces to viscous forces [23].

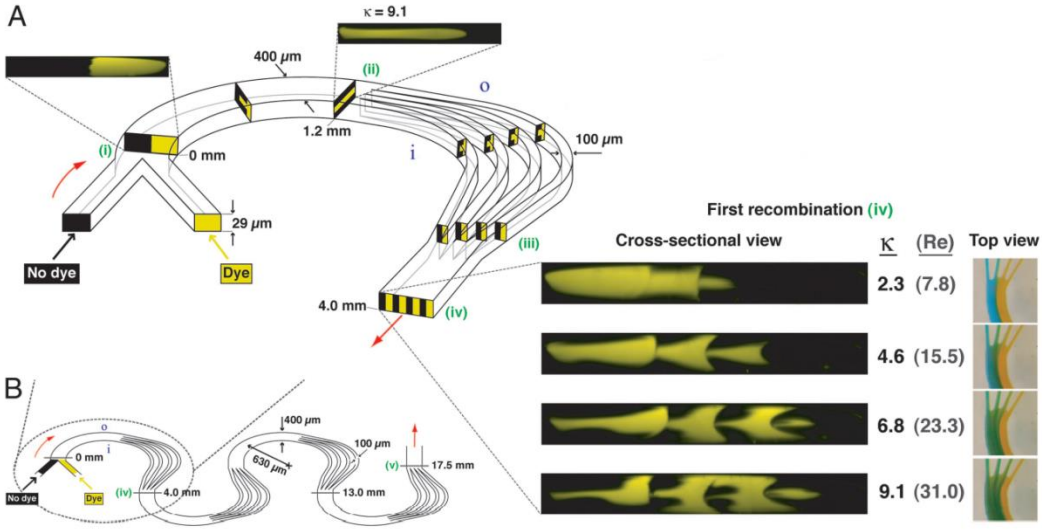

Figure 1.3. Sudarsan and Ugaz's micromixer design a) one mixing unit with representation of the flow inside the channels b) complete mixer [23].

Li and Chen [24] documented simplified version of their previously uncovered reversed flow micromixer. They proposed 3 possible micromixer designs to mimic the reversed flow characteristics of their initial design. They achieved to have over 80% mixing efficiency with all their design alternatives and reduce the pressure drop over a wide range (0.1-100) of Reynolds numbers [24]. Chen and Zhao [25] numerically worked on optimization of obstacle height and placement in a 3-D T micromixer. They uncovered that blockage of obstacles creates constant changes in flow velocity which creates chaotic advection. Their results revealed that the most important parameter affecting the performance of a micromixer is the obstacle height, followed by shape, number and symmetry of the obstacles. They designed a multi-unit micromixer and achieved 90% mixing efficiency [25]. Kwak et al. [26] investigated the herringbone type micromixers. They proposed a positive pattern herringbone application and compared their design with the traditionally used negative pattern herringbone micromixers, under forward and reverse flow conditions. Their results showed that the positive grooved herringbone micromixer with forward flow shows the best mixing [26]. Hoffmann et al. [27] designed a simple T-type micromixer and presented the fact that T-type micromixer is able to generate vortex structures even in laminar flow regimes very early in the literature.

They used micro-Laser-induced fluorescence to measure the mass transfer area and mixing efficiency [27]. Tsai and Wu [28] fabricated a microchannel that has two C shaped curved channels implemented with rectangular obstacles with a straight channel connection. With this design they benefitted from both Dean flow effect and chaotic advection originated from the baffles. They numerically studied the obstacle placement and obstacle height. The best results achieved when the first obstacle is located on the bottom wall of the micromixer at the entrance of the C shape channel and the second obstacle is placed inside the C shaped curve on the top wall of the micromixer 60^{o} apart from the first obstacle [28]. Çetkin and Miguel [1] designed a Y-shape micromixer and uncovered the effects of changing inlet channel angles, diameter and length ratios of outlet and inlet channels with constant volume constraint on mixing efficiency and pressure drop numerically. They investigated the effect of introducing a mixing chamber in between the inlet channels and outlet channel and obstacles inserted inside the outlet channel. They concluded that the introduced mixing chamber increases the mixing efficiency as well as the pressure drop and might be a good option for limited space applications because of its compactness compared to the simple Y- shaped mixer. Even though the obstacles introduced enhance the mixing they increase the pressure drop which makes their use unnecessary [1] . In their follow up study Çetkin and Miguel [29] investigated a 3-D design with mixing chamber to investigate the effect of additional angles for inlet channels in 3-D space and introduced eccentricity on the inlet channels. They also implemented obstacles inside the mixing chamber to further increase the mixing inside. Their results revealed that introduced obstacles decreased the mixing efficiency by blocking the swirling motion inside the chamber and increased the pressure drop. They also concluded that a mixer should be designed in 3-D space to be able to implement parameters such as eccentricity [29].

1.4. Fabrication of Microfluidic Devices

Fabrication of the microfluidic devices can be grouped in four parts; first the microchannels are fabricated using wafers and polymers, for example a common polymer used in microchannel fabrication is polydimethylsiloxane (PDMS) [30]. These

microchannels may have functional groups such as; micromixers, microsensors, reaction channels or microseperators, etc. Secondly these microstructures are sealed with appropriate bonding method like welding, gluing, etc. Then, produced microunits are attached to form a microfluidic device. In the fourth and last part the microfluidic device is integrated to the other laboratory equipment such as syringe pumps, energy sources, chemical reservoirs, etc. A sample microreactor is presented in figure 1.4 that is fabricated for production of droplet-based nanoparticles [3]. The microreactor in figure 1.4 involves two micromixers. At the start, the reagents filled and mixed in the first micromixer. Then the reaction occurs along the reactor. After the first reaction completed the third reagent is introduced to the system and mixed in the second micromixer then the process continues at the reaction 2 section.

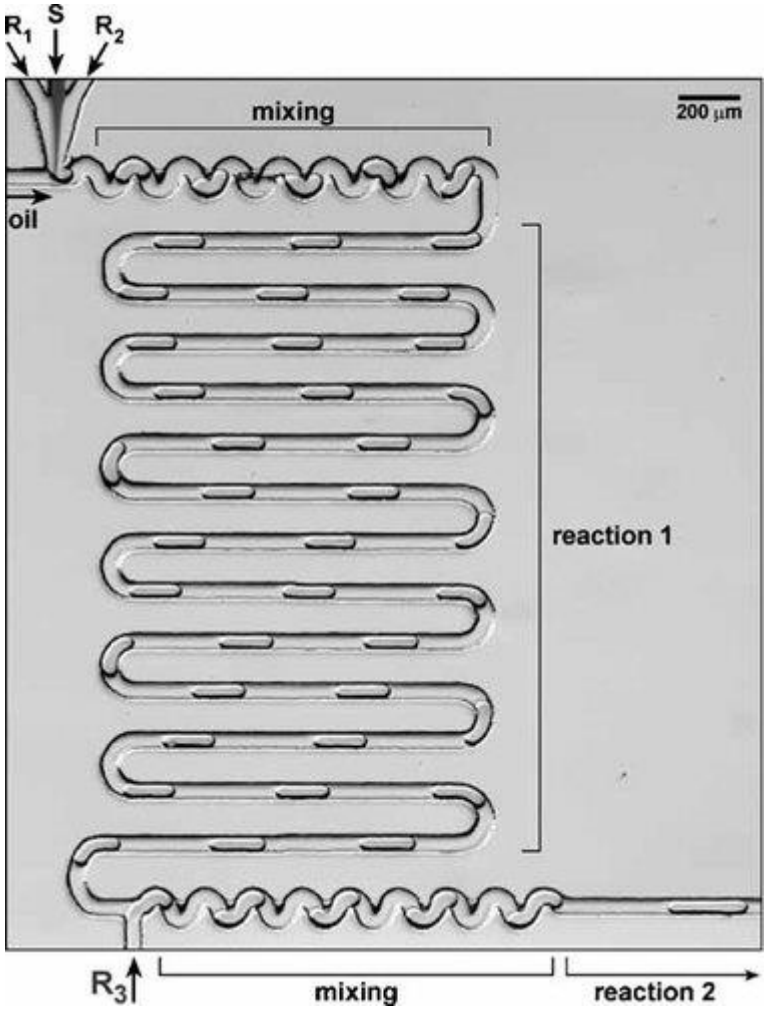

Figure 1.4. Micrograph of a microreactor for droplet-based nanoparticles [3]

Fabrication of microfluidic devices is still in development and many researchers are currently working on this subject [3 7 13 30]. Even though polydimethylsiloxane (PDMS) is widely used in fabrication of microfluidic devices, mixers, channels, etc., it fails to produce 3-D geometries and circular channels. Also, microchannel production with PDMS requires multiple production steps such as etching, patterning, curing, etc. [1330]. It is known that circular channels do not exhibit flow stagnation opposed to rectangular channels which is advantageous in cell immobilizing used in pharmacology industry. With circular channels, light transmission efficiency is enhanced and with 3-D geometries higher mixing efficiencies can be achieved [13 30]. These advantages motivate the researchers to work on both methods to fabricate 3-D geometries and circular channels using PDMS and investigate alternative microfabrication materials and methods. Zeraatkar, Tullio and Percoco [13] proposed to use additive manufacturing for fabrication of micromixers. They used fused filament fabrication (FFF) in their work for its biocompatibility, transparency and low-cost advantages. They also suggested that with fused filament method due to nature of the process, the produced micromixer already has ridges that enhance the mixing. They concluded that the mixer fabricated by 3-D printing with fused filament fabrication showed good mixing, however for high flow rates and channels wider than 0.6mm leakage is observed and the rough surface of the product might be a disadvantage for applications that requires smooth surfaces [13]. Abdelgawad et al. [30] proposed a method to produce circular microchannels with PDMS. They filled the rectangular PDMS channels with liquid PDMS and before it is cured air passed through the channel to blow out the liquid PDMS resulting in liquid PDMS to stick to the edges with surface tension and create a circular opening. Experimentations with this method uncovered that circular microchannels with varying diameters and sizes can be fabricated by adjusting the air velocity and the curing time [30]. Song et al. [31] used metal wire removing process to create circular microchannels. In this method the soldering wire is used to create a path for the microfluidic device, and then PDMS is covered over the soldering wire. After the PDMS is cured the soldering wire is melted away which leaves perfectly circular microchannels inside the PDMS mold. The limitation with this process is the minimum diameter of microchannels, a minimum diameter of 0.3mm is possible because of the available minimum soldering wire diameter [31].

1.5. Aim of Study

In this thesis, a parametric optimization study is conducted to uncover the effect of parameters on pressure drop and mixing efficiency for a 3-D Y-shaped micromixer design based on the work of Çetkin and Miguel's work [29] with mixing chamber and asymmetric inlet channels. Our aim is to while further optimizing the design, show its effectiveness among the already existing micromixers in the literature. For this purpose, the optimized micromixer design is compared with examples from literature with same boundary conditions (diffusion coefficient, Reynolds number, etc.) and same volume. The objective is to design the micromixer to either have the same mixing efficiency with lower pressure drop or having a higher mixing efficiency with same pressure drop, with the micromixer examples from the literature.

CHAPTER 2

METHOD

Two distinct micromixers were studied on COMSOL Multiphysics 5.4 [32] for their pressure drop and mixing efficiency results. The first micromixer is Tsai and Wu's CSC micromixer [28]. This micromixer is used for both validating the current study and present the other micromixer's developed performance. The other design is the Y-shaped micromixer that originated from Cetkin and Miguel's work [29] the length scale parameters are parametrically analyzed in order to uncover their effect on finding the maximum mixing efficiency and minimum pressure drop.

2.1. Simulation Parameters and Governing Equations

The simulation parameters and material properties are selected same as Tsai and Wu's work [28]. Single phase liquid water is set as the working fluids with constant properties and Rhodamine B is used as the soluble material inside the mixers. Working fluid density, viscosity and soluble material diffusion coefficient are 997 kg/m^3, 9.7×10^{-4}kg/m.s and 3.6×10^{-10} m^2/s, respectively. The Reynolds number is calculated as;

$$\mathrm{Re}=\bar{u} d_h \vartheta^{-1} \quad (2)$$

where $\bar{u}$ represents the mean outlet channel velocity, d_h represents the hydraulic diameter of the outlet channel and ϑ represents the kinematic viscosity.

The velocity distribution of the fluid flow inside the micromixer was calculated using conservation of mass (3) and momentum (4) equations. Steady state, laminar, incompressible and isothermal flow, with no-slip and impermeable wall assumptions were used in simulations. The simulations were conducted using quadratic discretization and the convergence criterion for relative tolerance was set to 10^{-3}. Velocity

distribution of the fluid flow inside the micromixer domain was calculated using equations (3) and (4). The velocity field data acquired from this calculation used in the convection-diffusion equation (5) to uncover the concentration distribution inside the micromixer domain. The equations used in the simulations are;

$$\nabla . u = 0 \tag{3}$$

$$\rho(u . \nabla) u = -\nabla P + \mu \nabla^2 u \tag{4}$$

$$u . \nabla c = D_c \nabla^2 c \tag{5}$$

Where u is velocity, P is pressure, μ is dynamic viscosity, ρ is density, D_c is diffusion coefficient and c is concentration.

For the calculation of mixing efficiency, method proposed in Çetkin and Miguel's work [29], presented in equation (6), is used.

$$M = 1 - \sqrt{\frac{\iint (\frac{c_i - \bar{c}}{\bar{c}})^2 dA}{\iint dA}} \tag{6}$$

In this method, normalized concentration difference, $[(c_i - \bar{c})/\bar{c}]^2$, is integrated over the interested cross-sectional area and divided to that cross-sectional area. Çetkin and Miguel [29] suggested that this method is superior to minimize errors in documenting mixing efficiency. Since the common mixing efficiency calculation methods use random or uniformly distributed data points that may lead to falsely reported results. The integration enables the distance between the data points become infinitesimally small that achieves a sensitivity level cannot be reached by limited number of sampling points. They also proved that this method yields more homogenous results, so this method is used in the rest of the study except when validating the current work.

In validation of the current study, the mixing efficiency is calculated using equation (7) and (8) that was used in Tsai and Wu's work [28]. The reason for using this method is to eliminate possible differences in mixing efficiencies that may be originated from different calculation methods. In Tsai and Wu's work [28] more traditional sampling point base approach was used. In this method the mole concentration fraction standard deviation is calculated on a cross sectional surface with equation (7), the concentration data is produced with uniformly distributed sampling points, then the result is inserted in equation (8) for the calculation of mixing efficiency.

$$\sigma^2 = \frac{1}{n} \sum_{i=1}^{n} (c_i - \bar{c})^2 \tag{7}$$

$$M = 1 - \frac{\sigma}{\sigma_0} \tag{8}$$

Pressure drop data for the micromixers were acquired from surface average module inside the COMSOL Multiphysics 5.4 software [32]. Average pressure values at the inlets of the micromixer were calculated with this module and the outlet pressure value is subtracted from the average inlet pressure value. The difference is documented as total pressure drop across the micromixer.

2.2. Numerical Models

2.2.1. CSC Micromixer

For the validation of the study, Tsai and Wu's CSC micromixer modeled on COMSOL Multiphysics 5.4 software as described in their article [28 32]. The working fluid is fed through the inlets with u velocity, which is calculated from the desired outlet Reynolds number, with c=0 mol/m^3 and c= 1 mol/m^3 molar distributions at either inlet as in figure 2.1. Pressure boundary condition is applied on the outlet as gauge pressure equals to 1 atm. The micromixer has a constant channel height of 130 μm. The inlet channels have a width of (W_i) 45 μm and length of (L_i) is 650 μm. For the rest of the micromixer channel width (W) is set to be 130 μm. The straight channel lengths connecting the inlet, the two mixing units and the outlet are; 260 μm, 390 μm and 1950 μm for the entrance region (L_e), for the straight connecting channel in between the two mixing units (L_c) and for straight outlet channel (L_o), respectively. The total calculated volume of the micromixer is 6.58×10^{-11} m^3. The curvature angle for the curved channels are set to 180^o and these are called mixing units. The obstacles inside the mixing units are placed as the first obstacle is on the inner surface of the mixing unit while the second obstacle is placed on the outer surface of the mixing unit with a 60^o separation angle. Obstacle width (W_b) and thickness (t) are 97.5 μm and 40 μm respectively. The CSC micromixer design is presented in figure 2.1.

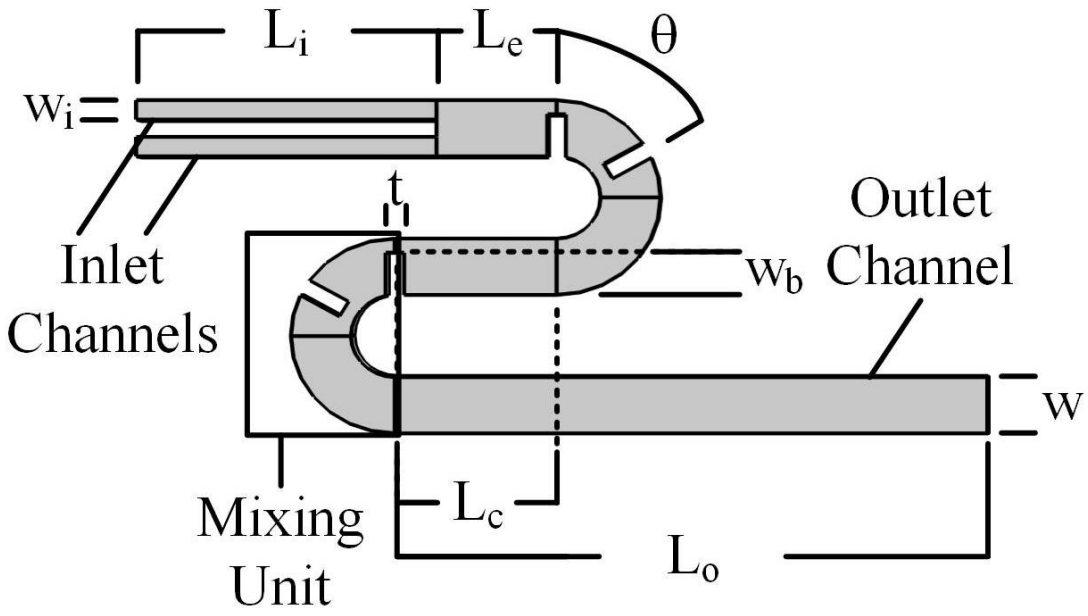

Figure 2.1. CSC micromixer design and dimension parameters.

2.2.2. Y-Shaped Micromixer with Mixing Chamber

A parametrical optimization study is conducted on the Y-shaped micromixer with mixing chamber design that is originated from Çetkin and Miguel's work [29]. The reagents are fed through the inlet channels with u velocity which is calculated based on desired Reynolds number in the outlet channel similar to the CSC micromixer section. The concentration distribution values are set as c=0 mol/m^3 at one and c= 1 mol/m^3 at the other inlet. Pressure boundary condition is set on the outlet as gauge pressure equals to 0 atm. Volume of the micromixer is set to 6.58×10^{-11} m^3 as same as the CSC micromixer. The boundary conditions, design and design parameters for the Y-shaped micromixer with mixing chamber are presented in figure 2.2.

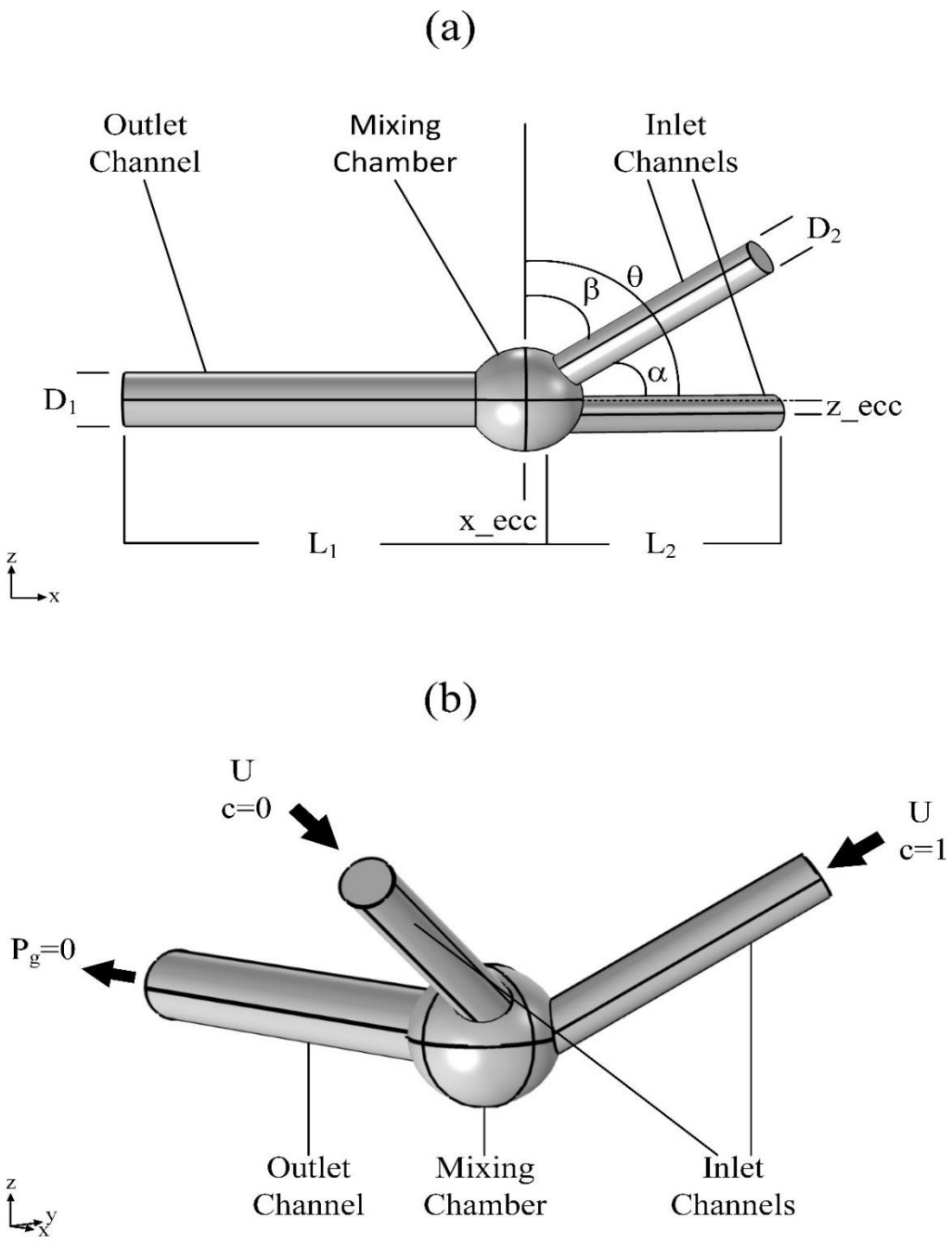

Figure 2.2. a) design parameters b) boundary conditions of the Y-shaped micromixer with mixing chamber.

In figure 2.2, beta (β) & theta (θ) are the angles between the inlet channels and the z axis on x-z plane. The θ angle is constant at 90^o. Alpha (α) is the angle between the two inlet channels on x-y plane. Z eccentricity is the distance between the centerline of an inlet channel and origin of the mixing chamber along z-axis, the distance between the two inlet channels centerlines is 2z. X eccentricity is the distance between the intersection point of the two inlets and the origin of the mixing chamber along x-axis. D_1, D_2, L_1 and L_2 are the diameter and length of the outlet and inlet channels respectively. Ratios of the outlet duct diameter to inlet duct diameter (D_1/D_2), outlet duct length to inlet duct length (L_1/L_2), inlet duct length to inlet duct diameter (L_2/D_2) and mixing chamber volume to total volume (V_{sp}) are parametrically investigated.

2.3. Mesh Independency and Validation Study

Varying mesh settings were surveyed for mesh independency. These settings created mesh element numbers from 21783 to 758668. Figure 2.3 presents the mixing efficiency results with corresponding number of mesh elements. It is possible to conclude from figure 2.3 that the mesh setting corresponding to 580607 mesh elements is sufficient for mesh independency. The relative error between this setting and the following denser mesh setting is in the order of 1%. In the rest of the study mesh setting generated 580607 mesh elements is used.

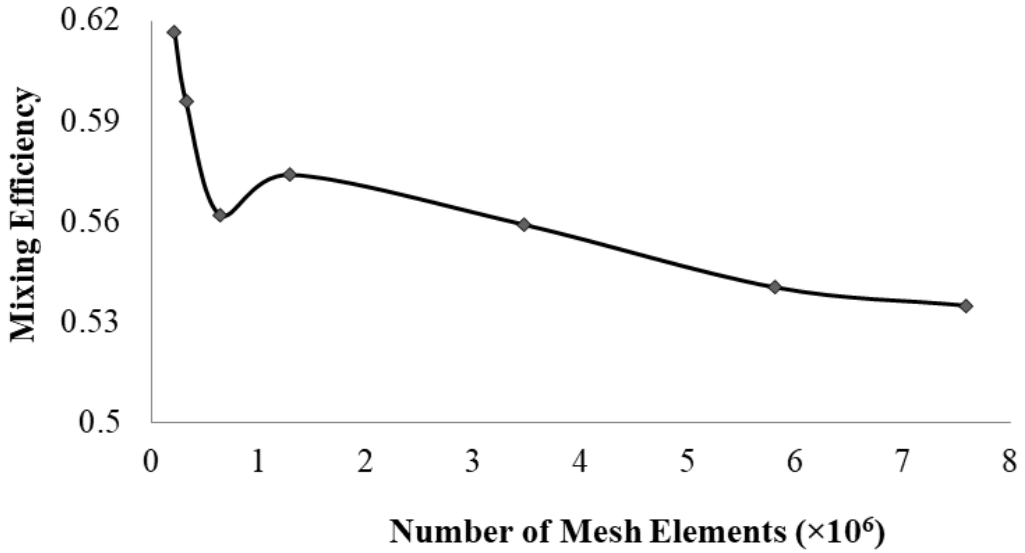

Figure 2.3. Change of mixing efficiency with different number of mesh elements for mesh independency study

The mesh setting that yields 580607 number of mesh elements is, for the domain: maximum element size 25.4 μm, minimum element size 7.5μm and maximum element growth rate 1.14. Denser mesh applied on the surfaces with settings; maximum element size 12.4 μm, minimum element size 1.4 μm and maximum element growth rate 1.1 and 5 layer boundary layer mesh is applied on the surfaces with 1.2 boundary layer stretching.

The selected mesh setting is applied to the CSC micromixer for validation. Results from the conducted simulations with the said mesh setting and reported in the Tsai and Wu's article [28] are presented in figure 2.4 for comparison. Results of Tsai and Wu's article are extracted by using Web Plot Digitizer [33]. In the graph, x-axis presents the Reynolds number on logarithmic scale and y-axis presents the mixing efficiency. Our simulated results and their reported results showed good agreement in trend and a maximum of 4% difference in between the mixing efficiency results are observed.

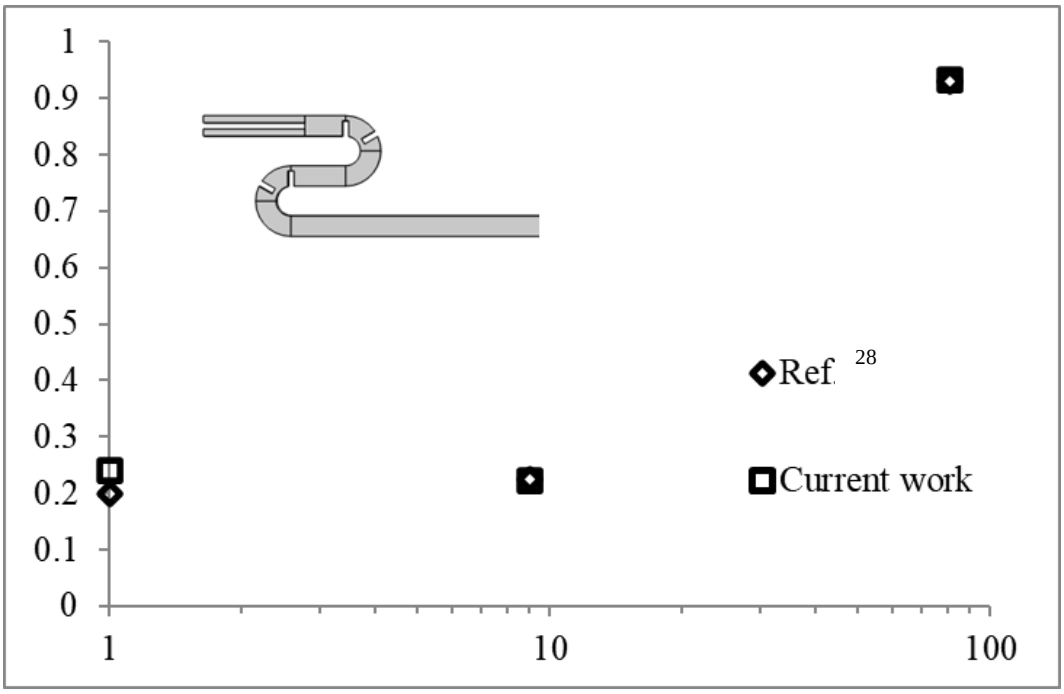

Figure 2.4. Comparison graph for reference article [28] and current work

CHAPTER 3

RESULTS AND DISCUSSION

In this part, optimization steps of the Y-shaped micromixer with mixing chamber that is first created in Çetkin and Miguel's article [29] are presented. Results of each step is given and discussed. Then performance comparison of the optimized design with reference design from the literature is made.

3.1. Optimization of α and β Angles with X and Z Eccentricities

The four parameters are investigated. The Reynolds number is set to 81 in the outlet channel and volume of the mixer is set to 6.58×10^{-11} m^3 same as the CSC micromixer. The other design parameters θ, L_1/L_2, D_1/D_2, L_2/D_2 and V_{sp} held constant at 90^o, 3, 1.4, 10 and 0.2 respectively. α parameter is studied in 0^o - 270^o angles range with 30^o angles increments, β angle is surveyed in 0^o - 90^o angles range with 30^o increments, x_{ecc} design parameter is investigated in between -20μm - 80μm range with 20μm steps and z_{ecc} design parameter is analyzed in between 0μm - 40μm range with 10μm steps. Presenting all the data from the survey of these four parameters in a single graph is not convenient because of the size of the data set. That is the reason that results are presented in five graphs containing mixing efficiency results for the α and β angles and x_{ecc} parameters for each z_{ecc} setting in figure 3.1.

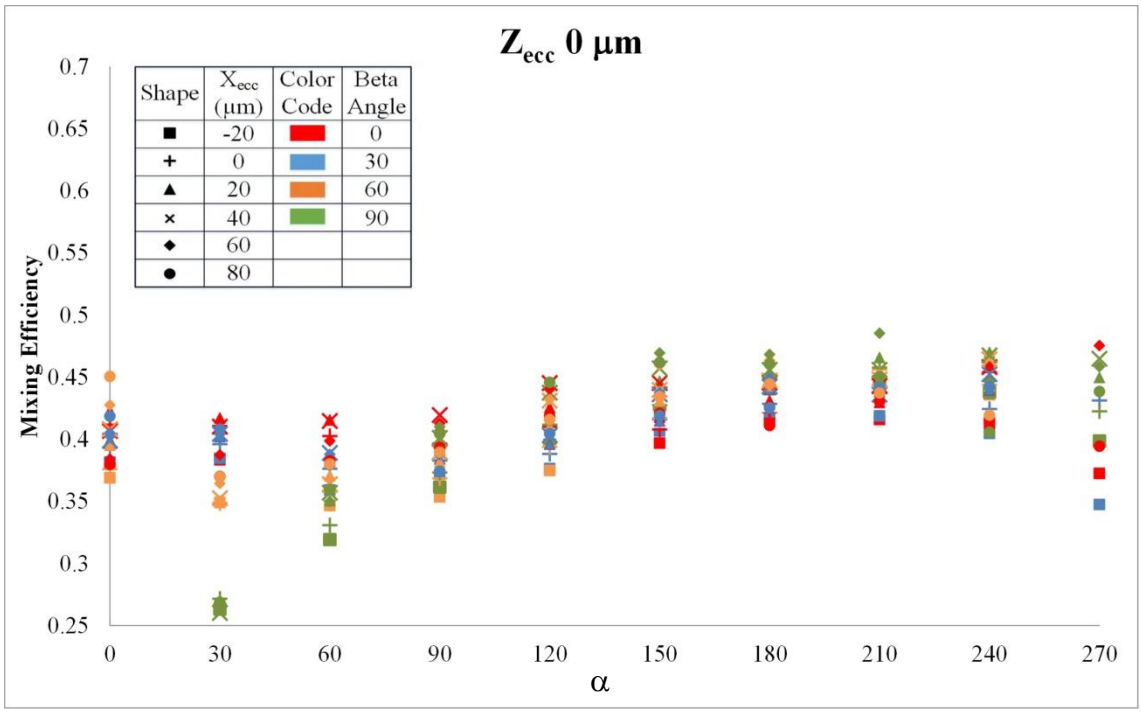

(a)

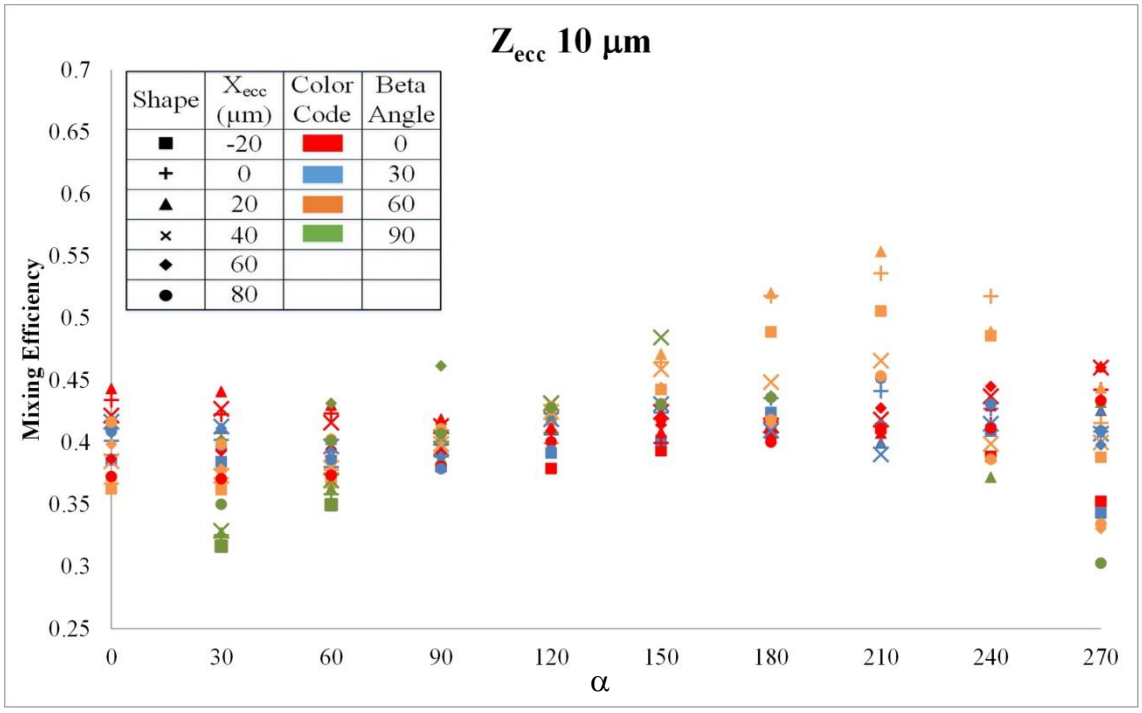

(b)

(cont. on next page)

Figure 3.1. Mixing efficiency results for the α and β angles and x_{ecc} parameters for a) z_{ecc}= 0µm b) z_{ecc}= 10µm c) z_{ecc}= 20µm d) z_{ecc}= 30µm e) z_{ecc}= 40µm

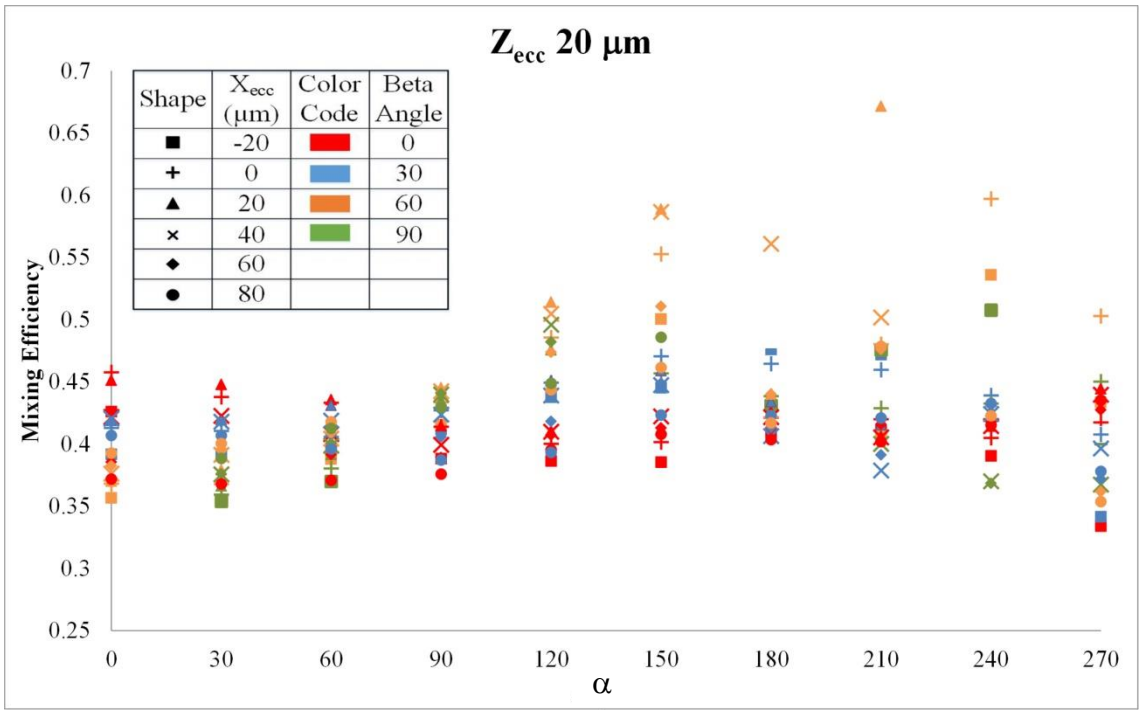

(c)

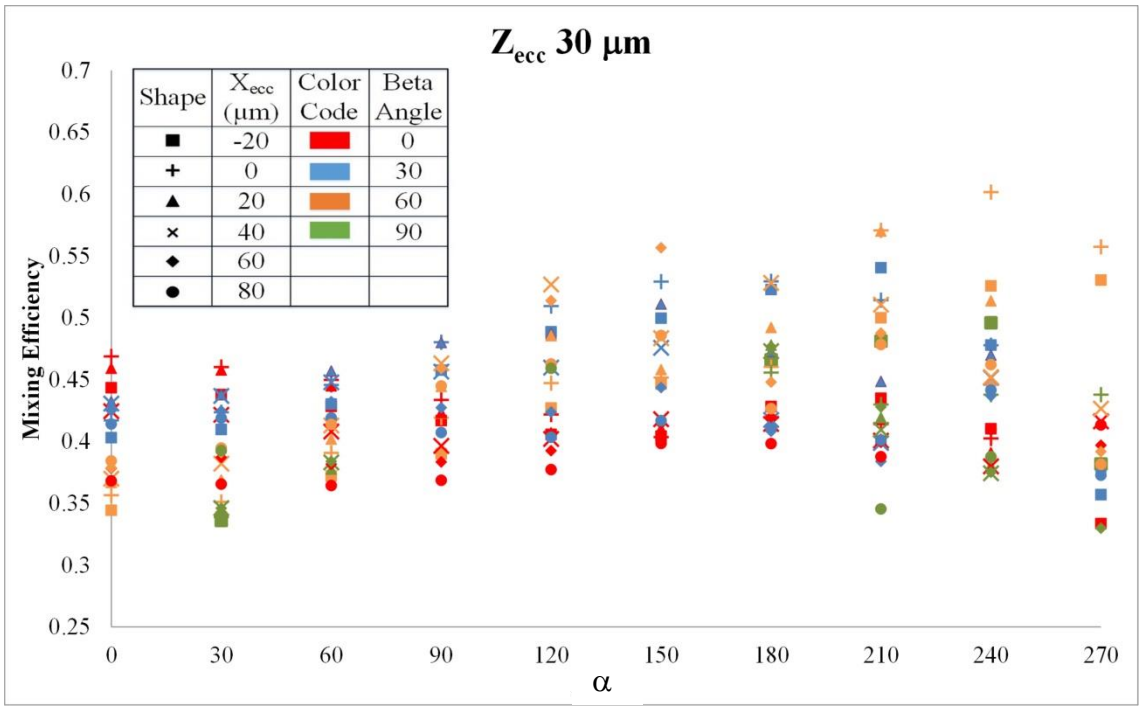

(d)

Figure 3.1 (cont.)

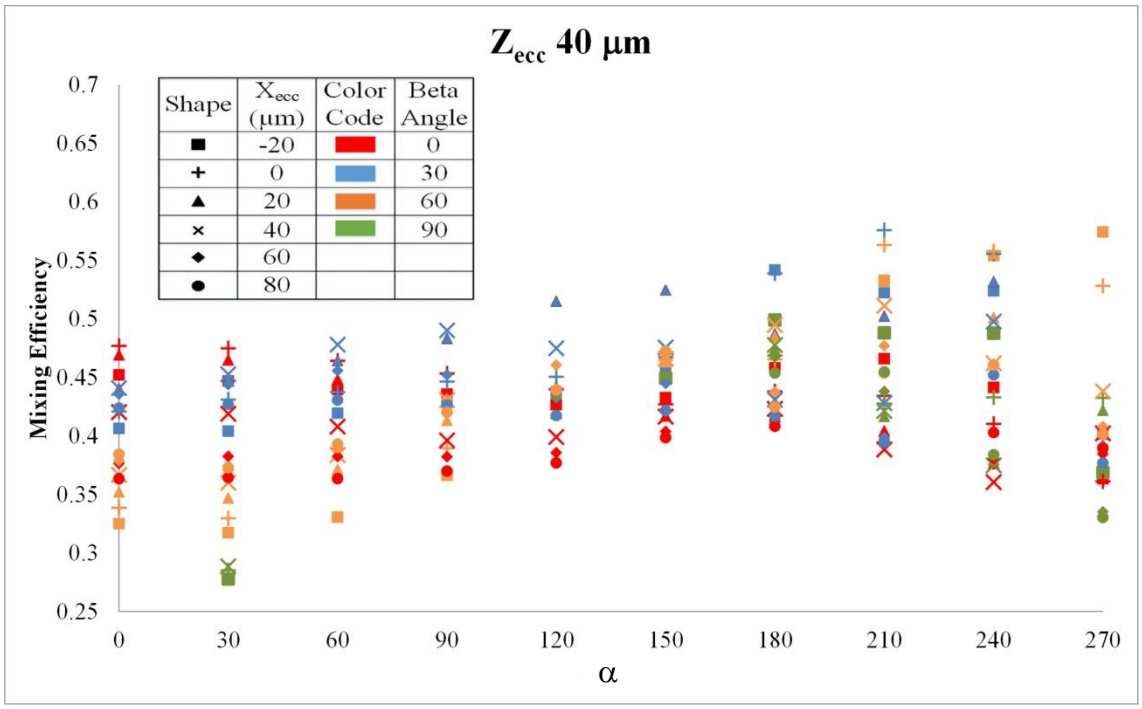

(e)

(Figure 3.1 cont.)

In figure 3.1, x-axis shows the α angles, y-axis shows the mixing efficiency (M) results, different colors represent the different β angle settings and different shapes represent the different x_{ecc} settings. When the figure 3.1 interpreted, it can be said that α angles in 180° to 240° range yield the highest mixing efficiencies. For the β angle it is not possible to show an optimum value or range because when results of β angles examined, for z_{ecc}= 0µm β= 90° followed by β= 0° yield the best results, however for the interval z_{ecc}= 10 - 30µm, β= 60° achieved the best mixing efficiencies. When z_{ecc} set to 40µm, β= 30° yield the highest efficiency results followed by β= 60°. Even though β= 60° configurations yield higher results when z_{ecc} introduced, it is believed that it is still not correct to suggest β= 60° is the best angle for this micromixer. For the x_{ecc} parameter a definite relation with the mixing efficiency could not be figured as well. Highest values of mixing efficiency achieved with x_{ecc}= 60µm for z_{ecc}= 0µm, x_{ecc}= 20µm for z_{ecc}= 10-20µm, x_{ecc}= 0µm for z_{ecc}= 30-40µm. It is possible to uncover a relation between the z_{ecc} parameter and the mixing efficiency. From figure 3.1 one can see that with introducing z_{ecc} to the system a sharp increase in maximum mixing

efficiency is occurring, however further increasing z_{ecc} after 20μm the maximum mixing efficiency values starts to decrease for all parameters. To sum up, it is possible to note that there is a clear relation between maximum mixing efficiency and α angle and z_{ecc} parameters. The optimum micromixer design should have α angle in 180° - 240° range and z_{ecc}= 20μm, however a conclusive result for β angles or x_{ecc} cannot be figured. It is thought that combinations of β angles and x_{ecc} parameters may be affecting the swirling motion or the chaotic advection inside the mixing chamber on multiple levels so that a simple curve that relates these parameters with the mixing efficiency cannot be constructed. For further investigation, it is decided to select the top three designs that yield highest mixing efficiencies, since it is not possible to construct a purely optimum micromixer with missing correlations for β angles or x_{ecc}. The design parameters for these designs are α= 210°, β= 60°, x_{ecc}= 20μm and z_{ecc}= 20μm for the design having the highest mixing efficiency (design 1), α= 240°, β= 60°, x_{ecc}= 0μm and z_{ecc}= 30μm for the second highest mixing efficiency (design 2) and α= 240°, β= 60°, x_{ecc}= 20μm and z_{ecc}= 20μm for the third highest mixing efficiency (design 3).

In this section the pressure drop caused by the designs is also calculated. The lowest and highest pressure drop calculated is found to be 4853.7 Pa and 5290 Pa. The mixing efficiency result of the design showing the lowest pressure drop is 35.4 %. This result is considerably lower than the maximum achieved mixing efficiency of 67.2 %. This 67.2% mixing efficiency required only 5097.1 Pa pressure drop. So 4.8% reduction on pressure drop causes 47.3 % loss in mixing efficiency. It is decided not to further investigate this minimum pressure drop design since the reduction of the pressure drop is insignificant compared to decrease in mixing efficiency.

Also, it should be noted that 10.8% of our cases resulted in non-convergence (130 cases out of 1200). It is believed that this is not critically important and has little effect on the outcome of this analysis. This situation may have been originated from using the steady state laminar flow module on COMSOL Multiphysics 5.4 software [32] and the solution to not to converge when complete steady state could not achieve or some local points to pass laminar region inside the swirling motion.

3.2. Optimization of V_{sp}, L_1/L_2, D_1/D_2 and L_2/D_2 Parameters

In this section V_{sp}, L_1/L_2, D_1/D_2 and L_2/D_2 are parametrically studied. The three best design configurations from the previous section further investigated with the following methodology. V_{sp} ratios from 0.1 to 0.9 are surveyed with 0.1 increments along with the other three design parameters. First, D_1/D_2 ratio is investigated from 1.2 to 2.0 with increments of 0.2 then L_1/L_2 parameter examined in between 2 to 6 with increment of 1 using the best D_1/D_2 ratio and at last the best configuration is searched through L_2/D_2 parameters from 8 to 12 with increments of 2.

3.2.1. Parametric Work on Design 1

3.2.1.1. Investigation of optimal D_1/D_2 ratio

The selected design 1 parametrically optimized. V_{sp} ratio is surveyed with varying D_1/D_2 ratios. Other parameters θ, L_1/L_2 and L_2/D_2 held constant at 90^o, 3 and 10 respectively. The results presented in figure 3.2.

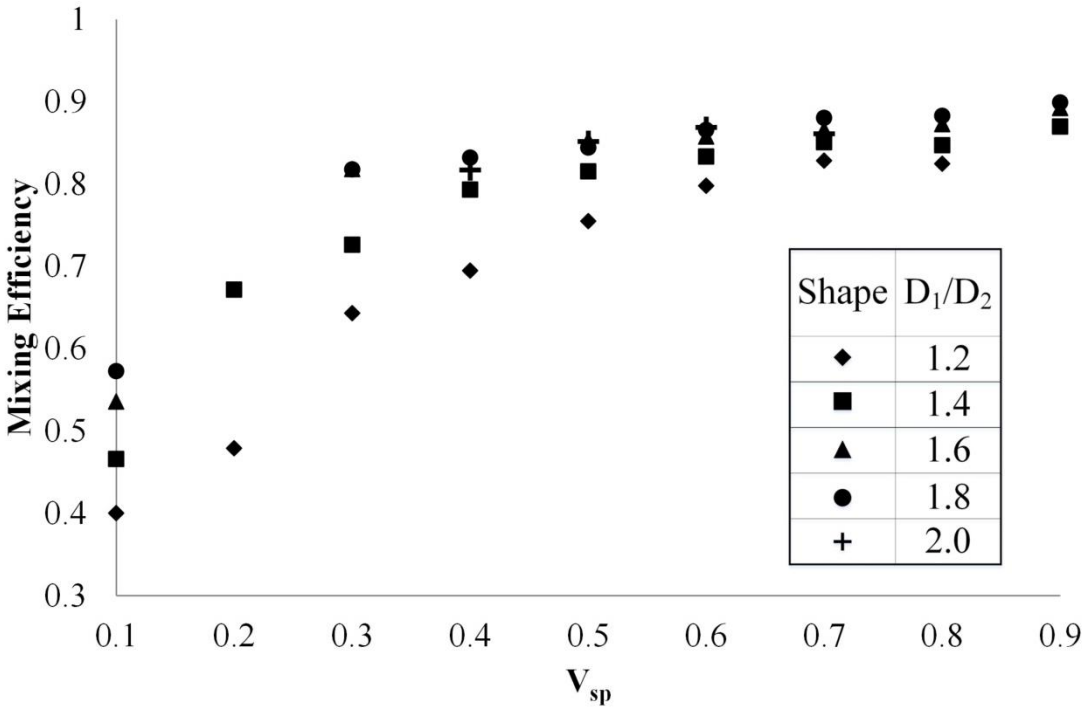

Figure 3.2. V_{sp} versus mixing efficiency graph for different D_1/D_2 ratios for design 1

In figure 3.2 it is visible that the highest mixing efficiency of 89.9% acquired with 0.9 V_{sp} and 1.8 D_1/D_2 ratios. The 1.8 D_1/D_2 ratio yield the highest mixing efficiencies in general. The increasing mixing efficiency with increasing D_1/D_2 ratio can be explained by the increase in outlet duct diameter enables fluid to rotate more freely inside the channel and results in enhanced mixing. The decrease in the mixing efficiency with 2.0 D_1/D_2 ratio is related with the constant volume constraint, increasing the outlet duct diameter results in shorter channel length which causes a reduction in the residence time of the fluid and mixing efficiency of the design. To sum up, decreasing benefits from increasing the outlet duct diameter and increasing disadvantage from the reduction of outlet channel length resulted with an optimum point at 1.8 D_1/D_2 ratio. In the graph there is a steep slope in mixing efficiency for V_{sp} values from 0.1 to 0.3, however the increase in the mixing efficiency slows down after further increasing V_{sp}. When the figure 3.3 is examined, it is possible to figure that this behavior is caused by insufficient mixing chamber volume. When the mixing chamber volume is not large enough, it fails to create a strong vortex inside the flow and forces the fluid to the outlet channel before sufficient mixing. As seen in figure 3.3 for V_{sp}= 0.1 the fluid exits the mixing chamber before being able to swirl in the chamber but in V_{sp}= 0.3 the fluid is

able to chaotically mix inside the mixing chamber before moving to the outlet channel. The slight increase after the 0.3 V_{sp} ratio can be explained by the fluid inside the mixing chamber experiencing a chaotic rotating flow for an increased time but since it already had enough volume the increase with increasing V_{sp} ratio is not as high as 0.1-0.3 region.

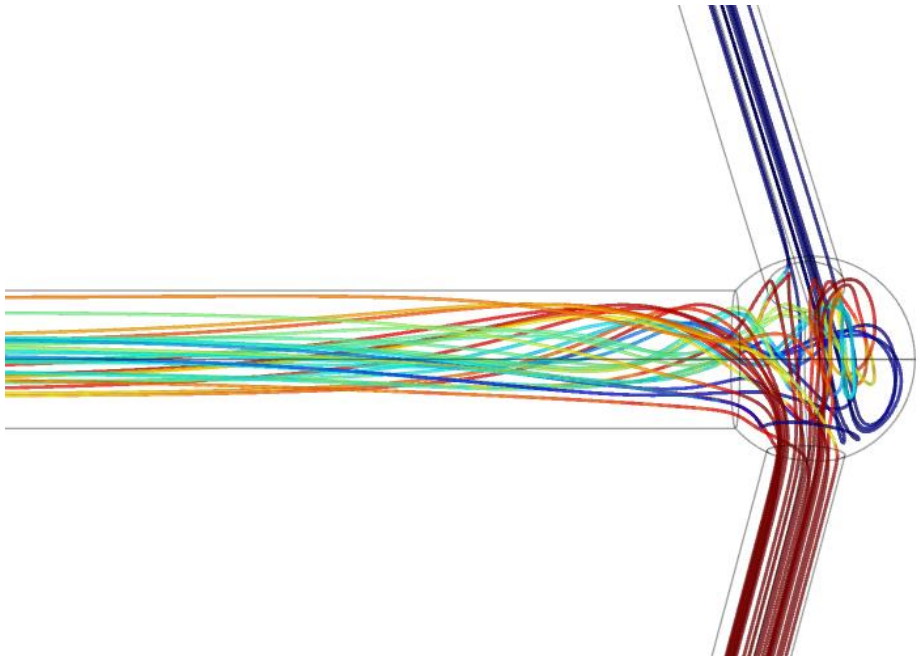

(a)

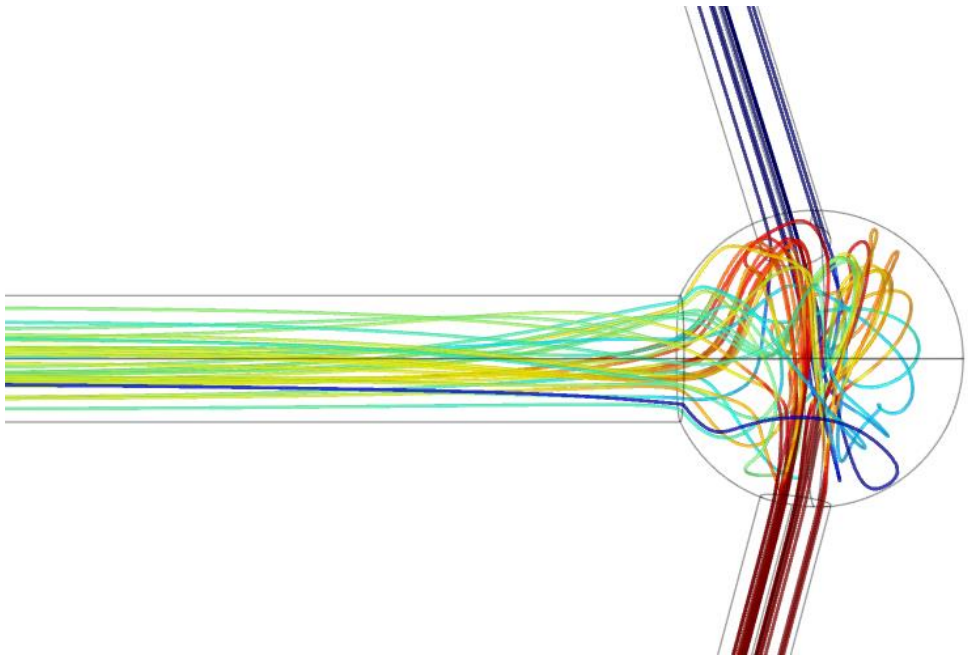

(b)

Figure 3.3. Concentration streamlines for a) V_{sp}= 0.1 b) V_{sp}= 0.3

The design achieved the highest mixing efficiency using 0.9 V_{sp} and 1.8 D_1/D_2 ratios caused the highest pressure drop of 13842 Pa, however design utilizing 0.3 V_{sp} and 1.8 D_1/D_2 ratios acquired 81.7% mixing efficiency with 5465.6 Pa pressure drop. This means 60.5% reduction in pressure drop can be achieved with sacrificing 9.1% mixing efficiency however design with 0.7 V_{sp} and 1.8 D_1/D_2 settings succeeded 88.0% mixing efficiency requiring 8157.6 Pa pressure drop and presents a good tradeoff. It should be noted that even though 0.9 V_{sp} ratio is yielding the highest mixing efficiency, this design is not very realistic. It is believed that 0.7 V_{sp} ratio represents a good limit for realistic design. In figure 3.4 0.9 V_{sp} and 0.7 V_{sp} is shown together for comparison.

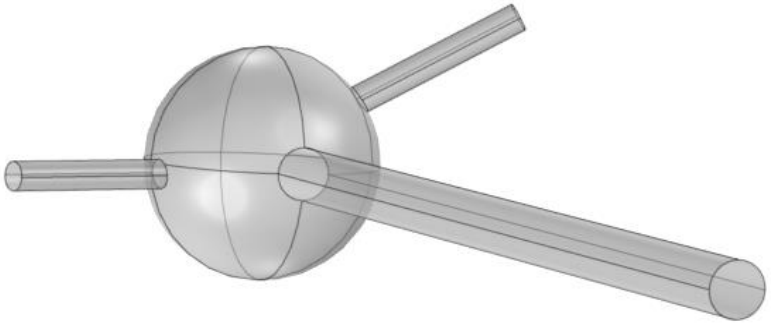

(a)

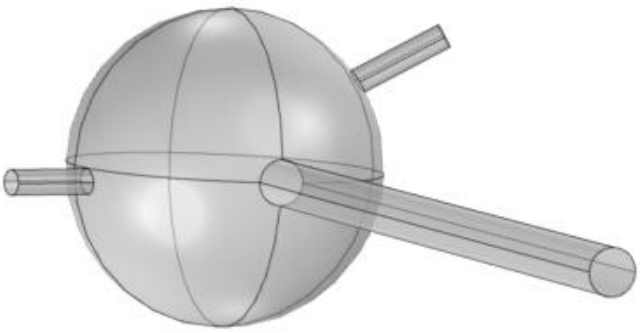

(b)

Figure 3.4. Design 1 with V_{sp} parameter equal to a) 0.7 b) 0.9

3.2.1.2. Investigation of optimal L_1/L_2 ratio

Design 1 is further evaluated for varying V_{sp} versus L_1/L_2 ratios with 1.8 D_1/D_2 applied. The other parameters θ, L_1/L_2 and L_2/D_2 held constant at 90°, 3 and 10 respectively. Results presented in figure 3.5.

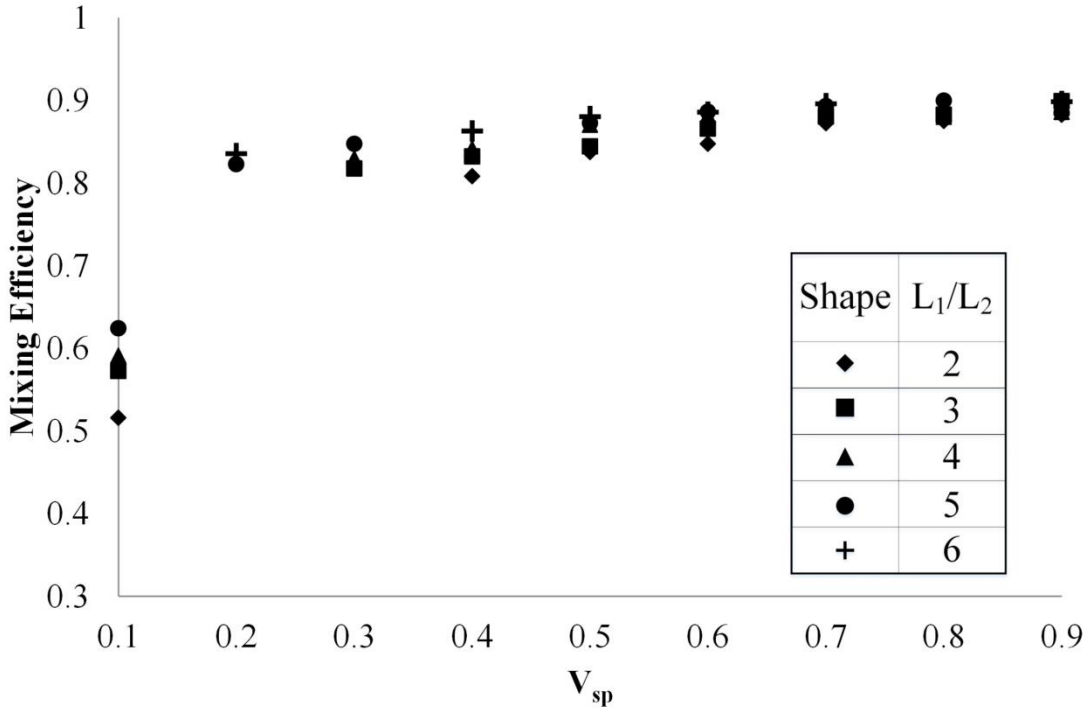

Figure 3.5. V_{sp} versus mixing efficiency graph for different L_1/L_2 ratios for design 1

Different L_1/L_2 ratios yield very close results. Even though it is possible to see the increase in mixing efficiency with increasing L_1/L_2 ratio, pressure drop increase related with it is significant. When the data is examined, L_1/L_2=4 ratio yields very close to the highest mixing efficiency values and achieves this mixing efficiency with significantly lower pressure drops. For example, for 0.5 V_{sp} design, with L_1/L_2=4 yields 87.0% mixing efficiency with 8223.1 Pa pressure drop where L_1/L_2=6 yields 88.0% mixing efficiency with 12541 Pa pressure drop. This means a 1.2% gain for mixing efficiency has a penalty of 34.4% for pressure drop. In the end it is decided to continue

with L_1/L_2= 4 parameter owing to its ability to achieve very close mixing efficiencies to the highest results with lower pressure drops.

3.2.1.3. Investigation of optimal L_2/D_2 ratio

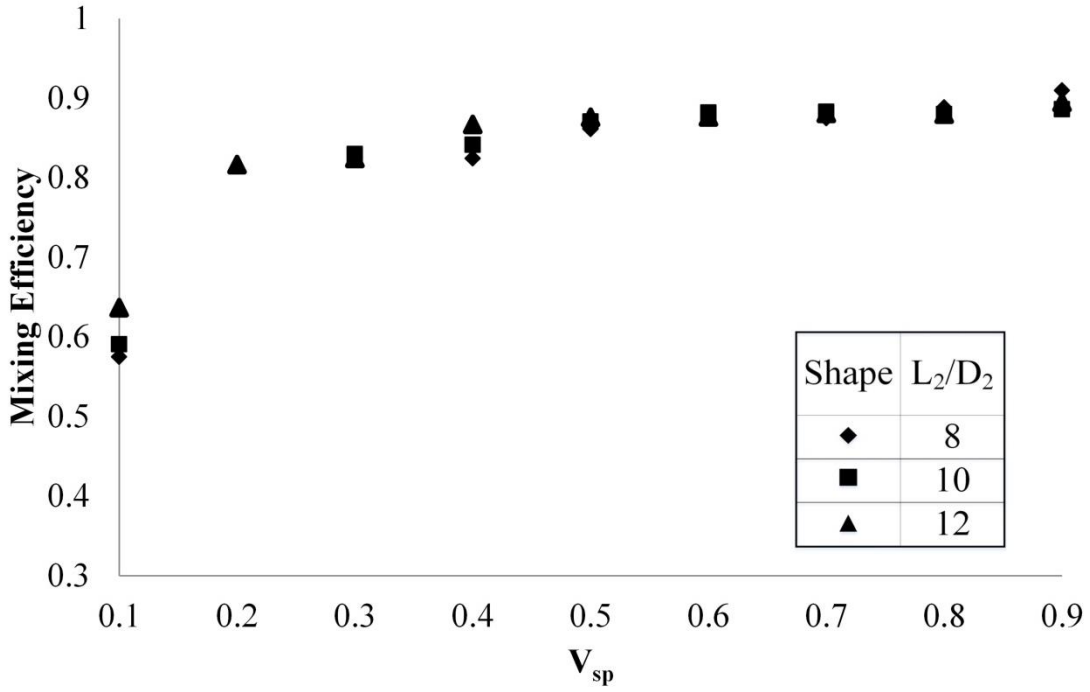

Figure 3.6. V_{sp} versus mixing efficiency graph for different L_2/D_2 ratios for design 1

Figure 3.6 shows that mixing efficiency results are nearly indistinguishable except for V_{sp} 0.1 and V_{sp} 0.4. This is because there is no mixing in the inlet channels so, length and diameter change of the inlet channels do not affect the system behavior considerably, however as L_2/D_2 ratio decreases the inlet channel length decreases resulting in a considerable decrease in pressure drop on the system. For example, for V_{sp} equals to 0.6, different L_2/D_2 ratios yield 87.59%, 88.16% and 87.63% mixing efficiencies with 6375.6 Pa, 9244.4 Pa and 12577 Pa pressure drops for L_2/D_2 equals to 12, 10 and 8 respectively. Even though lower L_2/D_2 ratio achieves lower pressure drop with almost no compromise, it is believed that further decreasing the L_2/D_2 ratio is not

meaningful since inlet channels are depended on the application. On account of that it is decided to continue with the initial L_2/D_2= 10 ratio in order not to falsely report a decrease on the pressure drop values, and not to further investigate this parameter.

In the end for design 1 selected values for the D_1/D_2, L_1/L_2 and V_{sp} are 1.8, 4 and 0.6 respectively. L_2/D_2 ratio is equal to 10 from this point on for all designs. V_{sp} 0.6 is selected because it can achieve almost the highest mixing efficiency 88.16% opposed to 88.59% mixing efficiency using V_{sp} 0.9 with a more realistic design and considerably lower pressure drop 9244.4 Pa opposed to 18314 Pa.

3.2.2. Parametric Work on Design 2

3.2.2.1. Investigation of optimal D_1/D_2 ratio

The selected design 2 studied parametrically. Varying D_1/D_2 ratios investigated for varying V_{sp} ratios. Other parameters θ, L_1/L_2 and L_2/D_2 held constant at 90º, 3 and 10 respectively. The results presented in figure 3.7.

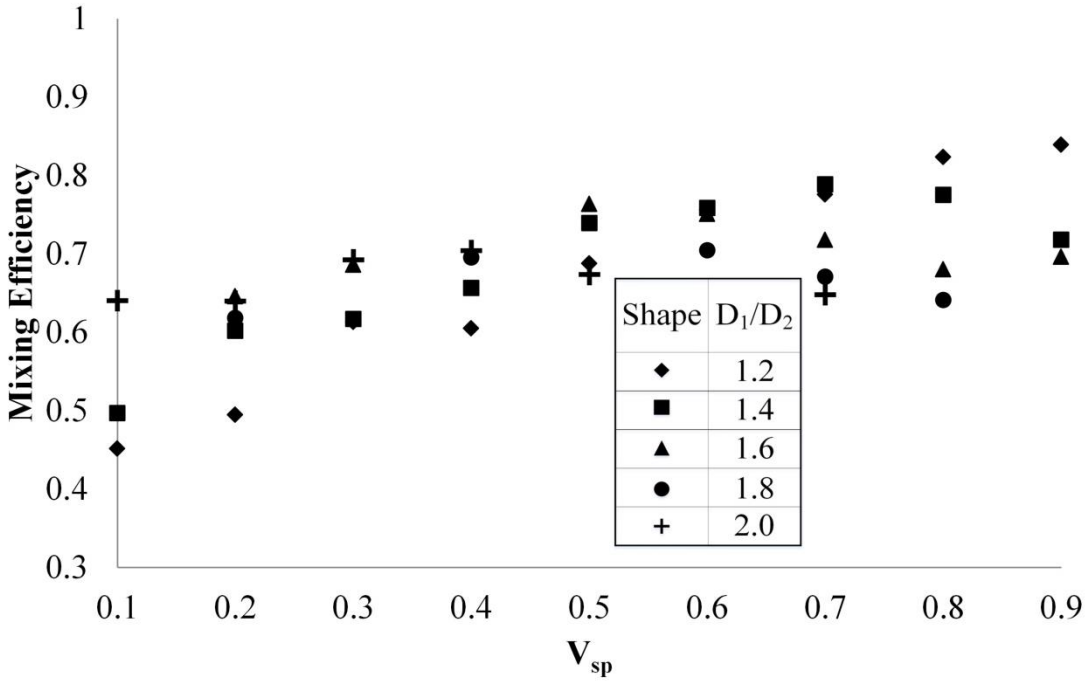

Figure 3.7. V_{sp} versus mixing efficiency graph for different D_1/D_2 ratios for design 2

The optimal D_1/D_2 ratio for this design is not obvious in figure 3.7. When examined, even though they did not yield the highest mixing efficiency, D_1/D_2 1.4 and 1.6 are the settings that provide consistently better results. It is decided to continue with the D_1/D_2 1.4 setting since D_1/D_2 1.6 has higher pressure drop levels compared to D_1/D_2 1.4 and does not have a significant advantage over it.

3.2.2.2. Investigation of optimal L_1/L_2 ratio

The design 2 further investigated for varying L_1/L_2 ratios and V_{sp} ratios. Other parameters θ, D_1/D_2 and L_2/D_2 held constant at 90°, 1.4 and 10 respectively. The results presented in figure 3.8.

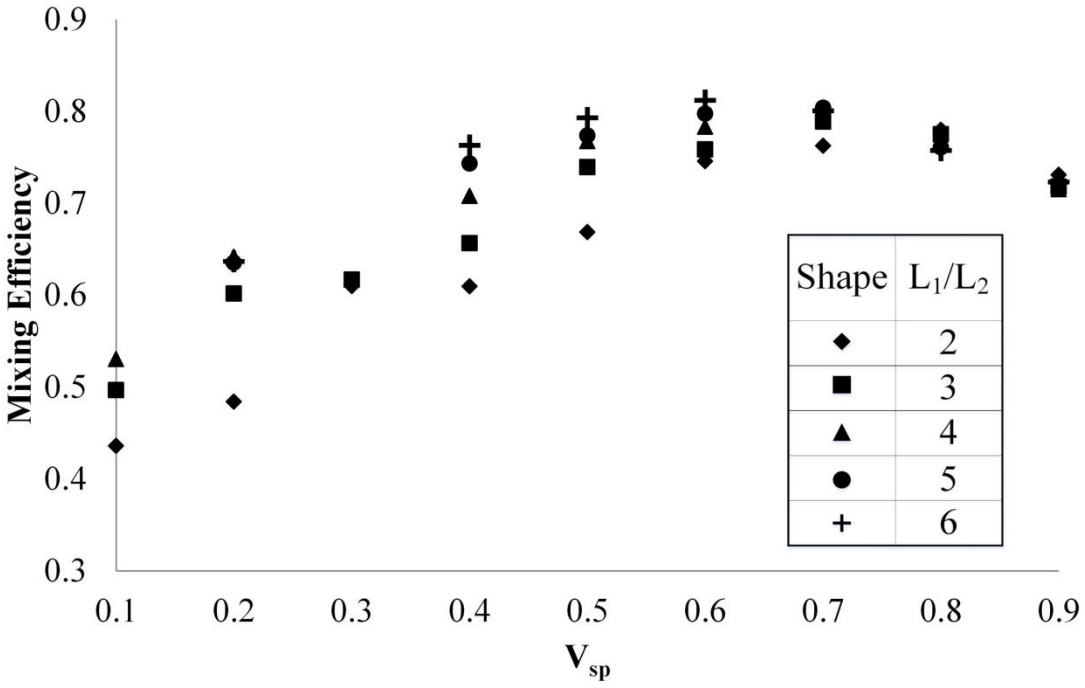

Figure 3.8. V_{sp} versus mixing efficiency graph for different L_1/L_2 ratios for design 2

When the figure 3.8 interpreted, it is possible to see that design 2 yielded its highest mixing efficiency with V_{sp} 0.6 and L_1/L_2 6 setting. Distinct increase in the mixing efficiency with increasing L_1/L_2 ratio and the decrease in mixing efficiency after V_{sp} 0.6 shows that design 2 is more depended on the outlet duct length than the design 1. This would mean that chaotic mixing in the mixing chamber of design 2 is not as significant as of design 1 so that design 2 needs longer outlet duct length to complete the mixing. Design 2 yields a maximum mixing efficiency of 81.19% with 16780 Pa pressure drop. This would mean that even if the pressure drops of the designs are not considered, design 2 is not capable of competing with design 1 and design 1 has very clear advantage over the design 2.

3.2.3. Parametric Work on Design 3

3.2.3.1. Investigation of optimal D_1/D_2 ratio

The design 3 is parametrically optimized. Varying D_1/D_2 ratios surveyed through different V_{sp} ratios. Remaining parameters θ, L_1/L_2 and L_2/D_2 held constant at 90°, 3 and 10 respectively. The results presented in figure 3.9.

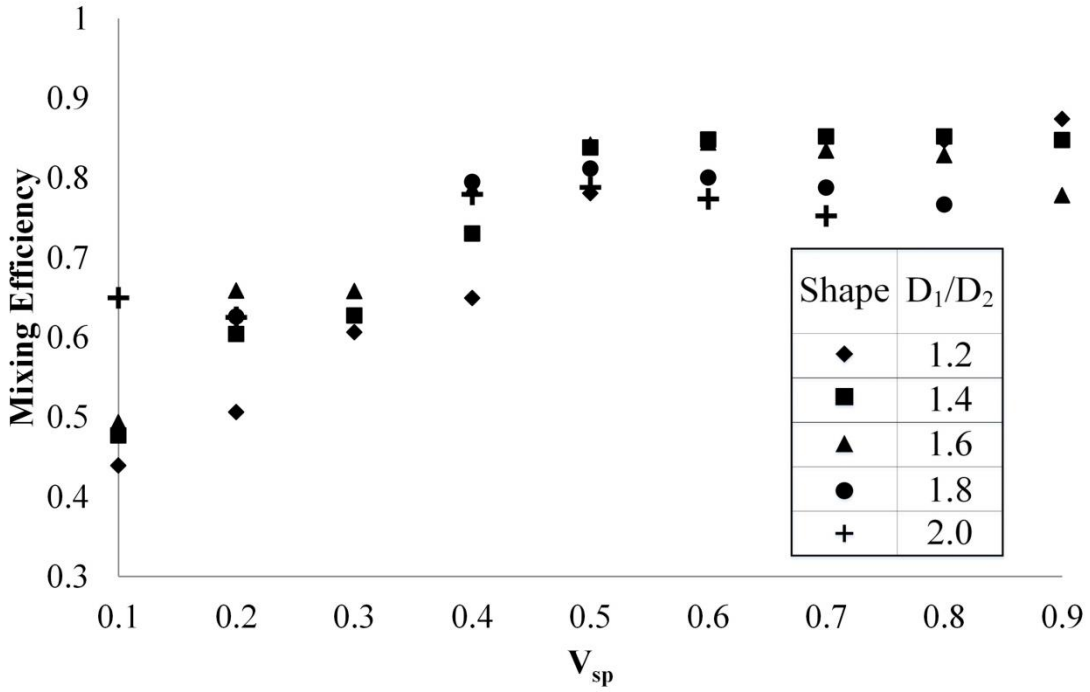

Figure 3.9. V_{sp} versus mixing efficiency graph for different D_1/D_2 ratios for design 3

In figure 3.9 the highest mixing efficiency attained by using, D_1/D_2 equal to 1.2 ratio with V_{sp} 0.9 ratio. However, considering unrealistic properties of V_{sp} 0.9 ratio and high mixing efficiencies achieved by D_1/D_2 1.4 and 1.6 ratios, it is clear that choosing D_1/D_2 1.4 or 1.6 ratio is more beneficial. D_1/D_2 1.4 and D_1/D_2 1.6 with V_{sp} 0.7 setting yield 85.17% and 83.42% mixing efficiencies and 8673.2 Pa and 8146 Pa pressure

drops respectively. Since D_1/D_2 1.4 reaches higher mixing efficiencies with very close pressure drops compared to D_1/D_2 1.6, it is decided to continue with this setting.

3.2.3.2. Investigation of optimal L_1/L_2 ratio

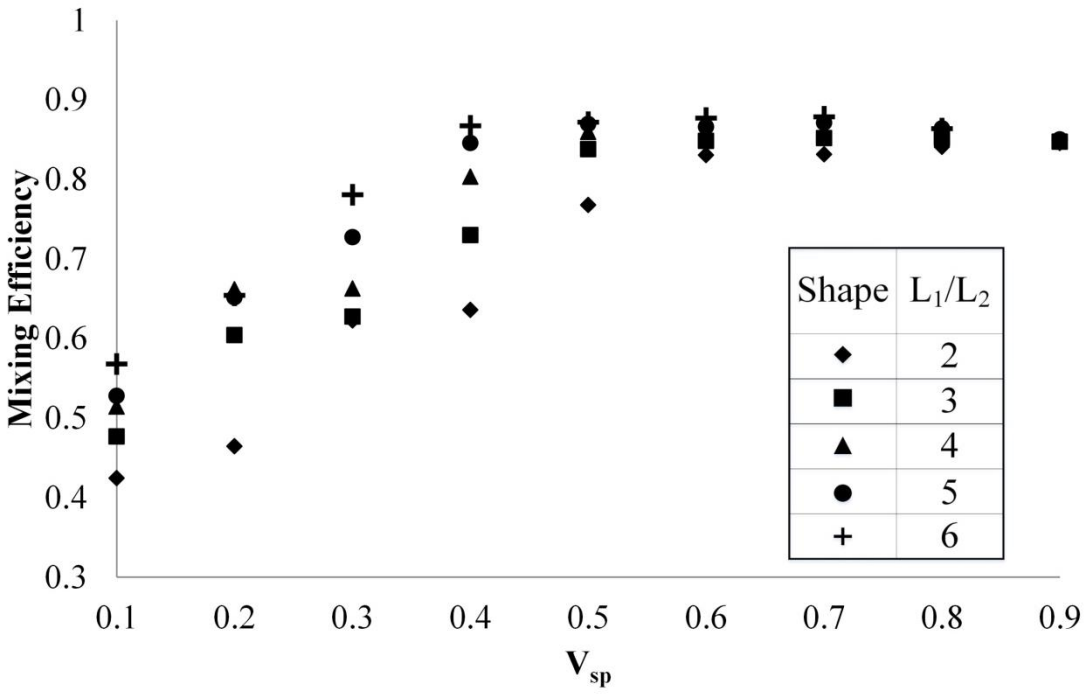

Figure 3.10. V_{sp} versus mixing efficiency graph for different L_1/L_2 ratios for design 3

Figure 3.10 shows that the highest mixing efficiency is acquired using L_1/L_2= 6 and V_{sp}= 0.7 configuration. For this setting the mixing efficiency is 87.83% and caused 16308 Pa pressure drop. The L_1/L_2= 6 ratio mostly achieved highest mixing efficiencies through this survey. The L_1/L_2= 5 ratio also achieved very close mixing efficiency results with L_1/L_2= 6 ratio. When the pressure drop values are investigated no significant difference could be observed. For example, for L_1/L_2= 6 and V_{sp}= 0.7 87.83% mixing efficiency with 16308 Pa pressure drop achieved where 87.11% mixing efficiency with 15732 Pa pressure drop achieved with L_1/L_2= 5 and V_{sp}= 0.7. There is an only 3.53% difference present between the pressure drops of the two settings which

is not significant. Because of the insignificant difference between the two highest yielding setting, L_1/L_2= 6 is selected as optimum value for design 3 due to its higher mixing efficiency.

When the optimum design 1 and design 3 is compared, their mixing efficiency and pressure drop values are 88.16% versus 87.83% and 9244.4 Pa versus 16308 Pa. Even though the mixing efficiency results of the two mixer setting are very close, there is a 43.31% difference between the pressure drops. It is very clear that the design 1 is more advantageous compared to design 2 and design 3.

3.3. Performance Investigation of the Optimized Design

Up to this point the Y-shaped micromixer design originated from Çetkin and Miguel's work [29] is optimized for its design parameters with constant 81 Reynolds number. In order to uncover the performance of the optimized micromixer at different Reynolds numbers the newly constructed design is simulated at 0.054, 023, 1, 3, 9 and 27 Reynolds numbers additional to the 81 Reynolds number. Mixing efficiency results for these Reynolds numbers are 94%, 51%, 24%, 19%, 18%, 49%, and 88% respectively. Contour plots of the outlet are given in the figure 3.11 for these Reynolds numbers.

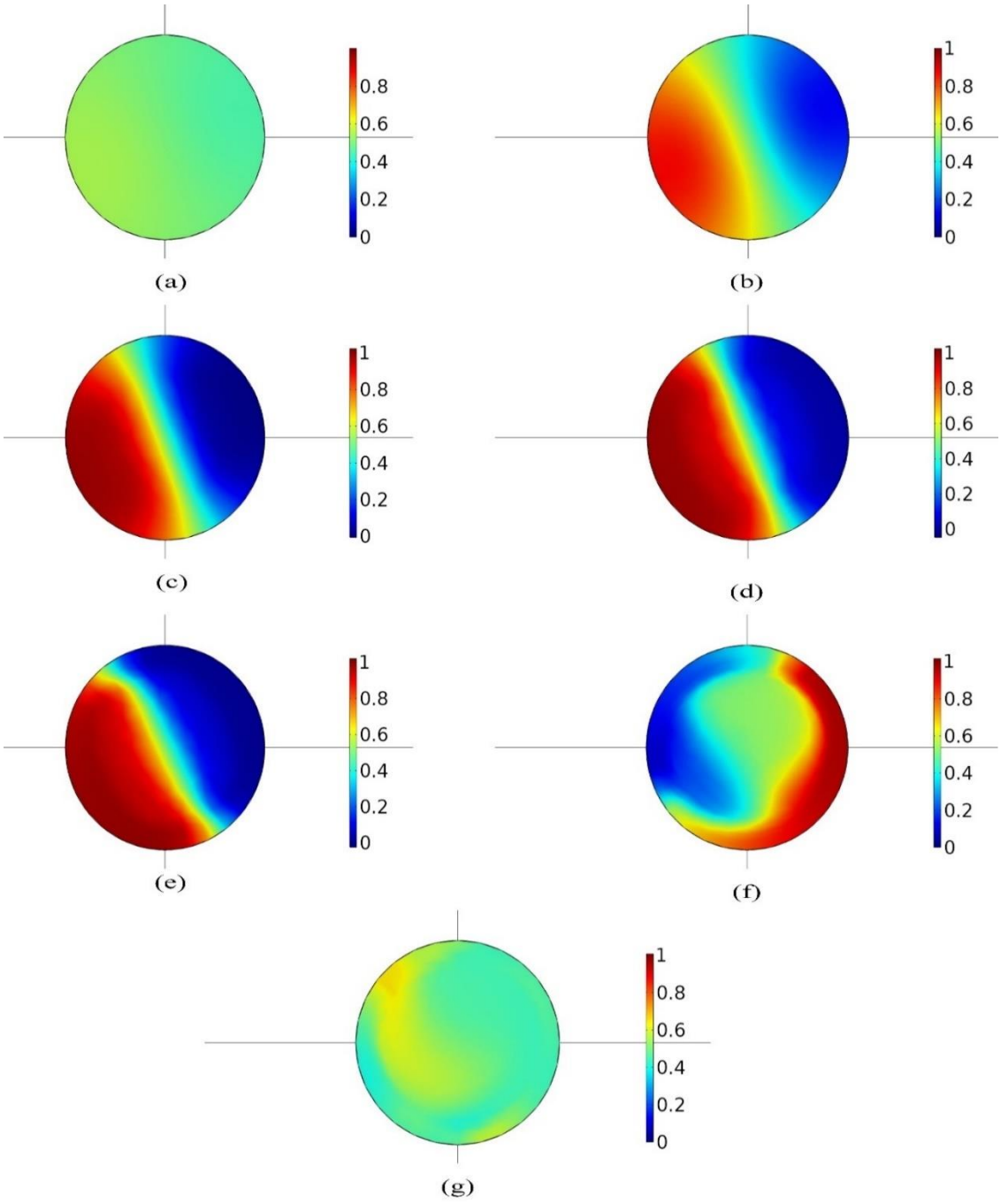

Figure 3.11. Outlet contour plots of the optimized design for Reynolds numbers a) 0.054 b) 0.23 c) 1 d) 3 e) 9 f) 27 g) 81

The mixing efficiency results and the contour plots show that the optimized design is performing well with very low and high Reynolds numbers. For low and intermediate Reynolds numbers performance of this mixer is not sufficient and this is visible in contour plots b-f. This result is expected since the Y-shaped micromixer with

mixing chamber that is optimized through this thesis is a chaotic mixer. Chaotic micromixers require high momentum fluid to create turbulent flow like structures. The low mixing efficiency results for Reynolds numbers 0.23-27 can be explained with this mechanism. In this interval while fluid do not have the enough momentum to initiate chaotic mixing, mean flow velocity inside the mixer is too high to enable mixing with pure diffusion. It is visible in contour plot b for Reynolds number 0.23, fluids are mixing with pure diffusion on the middle plane and no rotation exists inside the flow. Contour plot e for Reynolds number 9 shows that main mixing mechanism is still pure diffusion and flow is too fast to be able to mix with this mechanism, but flow shows some rotation which suggest that increasing Reynolds number will increase the mixing efficiency from this point. For Reynolds number 0.054 high mixing efficiency achieved even with the absence of high momentum is simply resulted from the increase residence time inside the micromixer. Increase in mixing efficiency after Reynolds 27 simply suggest that the momentum of the working fluid is starting to be sufficient for chaotic mixing. The rotation of the fluid for after 27 Reynolds number regime is also visible in the contour plots given in figure 3.11.

3.4. Comparison of the Optimal Design with another Micromixer

In this part the optimized micromixer with the selected parameters (design 1) is compared with Tsai and Wu's CSC micromixer [28]. Aim of this part is to show the performance of the optimized micromixer by showing it can attain comparable mixing with the other examples while having lower pressure drop values.

3.4.1. Detailed Comparison with the CSC Micromixer

Performance of the studied optimized micromixer is compared with the reported performance of the CSC micromixer that was also used in validation. Mixing efficiency and pressure drop values for the micromixers are presented in table 3.1. In the table

mixing efficiency and pressure drop results of the CSC micromixer and the studied design with optimized parameters (design 1) is given side by side. The results for mixing efficiencies and pressure drops of the CSC micromixer for different Reynolds numbers are acquired using Web Plot Digitizer [33]. Relative differences of the mixing efficiency and pressure drop values also given in the right-hand side of the table. Relative differences calculated as in equation (8).

$$\frac{X_{csc}-X_{our}}{X_{csc}} \quad (8)$$

In equation (8) X represents the interested parameter and subscripts csc and our represents the CSC micromixer and the optimized Y-shaped micromixer with mixing chamber respectively.

Table 3.1. CSC micromixer versus optimized Y-shaped micromixer

	CSC Micromixer [28]		Optimized Design		Variation %	
Reynolds Number	Mixing Efficiency	Pressure Drop (Pa)	Mixing Efficiency	Pressure Drop (Pa)	M_{eff}	P_{drop}
0.054	0.94	11.36	0.94	5.46	0	51.94
0.23	0.5	47.62	0.51	23.26	-2	51.15
1	0.2	210	0.24	101.15	-20	51.83
3	0.14	630.96	0.19	303.49	-35.71429	51.90
9	0.22	1944.86	0.18	911.87	18.18182	53.11
27	0.54	6984.47	0.49	2797.1	9.259259	59.95
81	0.93	33282.98	0.88	9244.4	5.376344	72.22

The table 3.1 shows that more than 50% pressure drop reduction is possible with using the optimized Y-shaped micromixer design instead of the CSC micromixer for all Reynolds numbers. For Reynolds numbers lower than or equal to 3, the optimized micromixer offers up to 35.58% higher mixing efficiency results with 51.90% power save. For Reynolds numbers 9 27 and 81 optimized design could not reach the mixing efficiency values attained by the CSC micromixer. The selected design 1 caused 17.28%, 8.90% and 5.21% reduction in mixing efficiencies for Reynolds numbers 9 27 and 81 respectively however, the 53.11%, 59.95% and 72.22% reduction in pressure

drops for the same Reynolds numbers that is attained by using the optimized design should be considered. This would mean that, it is theoretically possible to connect two of the optimized micromixers to a system and achieve a lower pressure drop value than using one CSC micromixer.

When the trend in table 3.1 shows that as the Reynolds numbers increase from 9 to 81 the difference in mixing efficiencies between the CSC micromixer [28] and our optimized design decreases while the difference between the pressure drops of these two designs increases. This would suggest the optimized design 1 may perform better than CSC micromixer [28] when higher Reynolds numbers considered.

All in all, our design offers better mixing while achieving considerable pressure drop reduction for low Reynolds numbers (0.054-3). In the transition region and at beginning of the high Reynolds numbers CSC micromixer [28] surpasses our micromixer when mixing efficiency is considered, however there is still a significant (more than 50%) decrease on pressure drop acquired by our optimized design. This is because, in transition region the fluid does not have enough momentum to start the chaotic advection or the swirling motion inside the mixing chamber however, it is not slow enough to increase the residence time in the mixer to achieve mixing with pure diffusion which causes poor mixing. The decreasing difference between the mixing efficiencies and enhancing reduction on pressure drop with increasing Reynolds numbers suggest that for high Reynolds number regime the optimized Y-shaped micromixer design can surpass the CSC micromixer [28] on achieved mixing efficiency results while obtaining over 70% pressure drop reduction through the mixer.

CHAPTER 4

CONCLUSION

In this thesis general information about the application fields, purpose and mixing mechanism of the micromixers is given. Some microfluidic applications are surveyed to uncover the importance of micromixers for microfluidic devices. Working principle, advantages and types of micromixers (active and passive) are presented with examples from the literature. Fabrication processes and methods, for microfluidic devices are explained and the importance of micromanufacturing 3-D structures for these devices expressed.

A Y-shaped micromixer with mixing chamber that has 3-D geometrical properties was investigated and parametrically optimized. 3-D geometry enabled us to study the effects of x eccentricity, z eccentricity and provided a wider range for the design of inlet channels. When the different settings for inlet angles and eccentricities surveyed, it is found that α angles attain highest mixing efficiencies in 180^o to 240^o range and z_{ecc}= 20μm represents a good optimal value. However, for β angle and x_{ecc} an optimal value or a range could not be uncovered. Consequence of that, instead of setting a new optimal design with individual optimal parameters the highest yielding top three designs investigated through this thesis.

Later, the Y-shaped micromixer with mixing chamber is investigated for V_{sp}, L_1/L_2, D_1/D_2 and L_2/D_2 parameters. It is found that a general trend for V_{sp} parameter exists, as this parameter increases the mixing efficiency enhances, however after V_{sp} 0.7 the design does not considered very realistic. The simulations showed that optimum values for parameters L_1/L_2 and D_1/D_2 are dependent on the other design parameters, so the selected values for them are different for each design alternative. L_2/D_2 parameter showed almost no effect on mixing efficiency. Although L_2/D_2 had considerable effect on pressure drop it is decided not to investigate this parameter as reducing pressure drop by shortening the inlet channels is not realistic since the inlet channel length is dependent on the application in real life.

The parametric work uncovered that the design 1 (α= 210^o, β= 60^o, x_{ecc}= 20μm and z_{ecc}= 20μm) with V_{sp}, L_1/L_2, D_1/D_2 and L_2/D_2 equal to 0.6, 4, 1.8 and 10 respectively, can be considered as the optimized design. Since it achieves nearly the highest mixing efficiency of 88.16% with relatively low 9244.4 Pa pressure drop.

In the following, this selected optimized design is compared with the base design (CSC micromixer [28]). This comparison revealed that our micromixer design can attain mixing efficiencies up to 35.58% higher than base design for low Reynolds numbers (0.054-3). The optimized micromixer design can achieve over 50% reduction on pressure drop for all Reynolds numbers where a maximum reduction 72.22% on pressure drop is observed when Reynolds number is 81. When the trend in table 3.1 interpreted, it can be assumed that the optimized Y-shaped micromixer can obtain higher mixing efficiencies while requiring considerably lower pressure drops compared to CSC micromixer [28] for high Reynolds numbers after the transition regime. In transition regime our micromixer fails to surpass the mixing efficiency values of CSC micromixer [28]. The reason for this situation is that the working fluid not having enough momentum in this regime to start chaotic advection inside the mixing chamber. However, it is important to note that the Y-shaped micromixer keeps achieving over 50% decrease in pressure drop.

All in all, in this work Y-shaped micromixer with mixing chamber parametrically optimized for acquiring high mixing efficiencies with low pressure drops. Results revealed that sufficient mixing can be attained with this micromixer while succeeding significant decrease in pressure drop. This suggests that this micromixer can be useful for systems that require very compact design and significantly low pressure drops.

For the future studies, in this thesis experimental study could not be conducted, this micromixer should be experimentally tested, compared to more micromixers in the existing literature and a more planar design having the similar properties can be examined for easier fabrication.

REFERENCES

(1) Cetkin, E.; Miguel, A. F. Constructal Branched Micromixers with Enhanced Mixing Efficiency: Slender Design, Sphere Mixing Chamber and Obstacles. Int J Heat Mass Transf 2019, 131, 633–644. https://doi.org/10.1016/j.ijheatmasstransfer.2018.11.091.

(2) Yuan, S.; Jiang, B.; Jiang, F.; Drummer, D.; Zhou, M. Numerical and Experimental Investigation of Mixing Enhancement in the Passive Planar Mixer with Bent Baffles. *Int J Heat Mass Transf* **2022**, *191*. https://doi.org/10.1016/j.ijheatmasstransfer.2022.122815.

(3) Song, Y.; Hormes, J.; Kumar, C. S. S. R. Microfluidic Synthesis of Nanomaterials. *Small*. June 2008, pp 698–711. https://doi.org/10.1002/smll.200701029.

(4) Damiati, L. A.; El-Yaagoubi, M.; Damiati, S. A.; Kodzius, R.; Sefat, F.; Damiati, S. Role of Polymers in Microfluidic Devices. *Polymers (Basel)* **2022**, *14* (23), 5132. https://doi.org/10.3390/polym14235132.

(5) Liu, M.; Xiang, Y.; Yang, Y.; Long, X.; Xiao, Z.; Nan, Y.; Jiang, Y.; Qiu, Y.; Huang, Q.; Ai, K. State-of-the-Art Advancements in Liver-on-a-Chip (LOC): Integrated Biosensors for LOC. *Biosens Bioelectron* **2022**, *218*, 114758. https://doi.org/10.1016/j.bios.2022.114758.

(6) Arora, A.; Simone, G.; Salieb-Beugelaar, G. B.; Kim, J. T.; Manz, A. Latest Developments in Micro Total Analysis Systems. *Anal Chem* **2010**, *82* (12), 4830–4847. https://doi.org/10.1021/ac100969k.

(7) Chen, P.; Chung, M. T.; McHugh, W.; Nidetz, R.; Li, Y.; Fu, J.; Cornell, T. T.; Shanley, T. P.; Kurabayashi, K. Multiplex Serum Cytokine Immunoassay Using Nanoplasmonic Biosensor Microarrays. *ACS Nano* **2015**, *9* (4), 4173–4181. https://doi.org/10.1021/acsnano.5b00396.

(8) Glawdel, T.; Elbuken, C.; Lee, L. E. J.; Ren, C. L. Microfluidic System with Integrated Electroosmotic Pumps, Concentration Gradient Generator and Fish Cell Line (RTgill-W1)—towards Water Toxicity Testing. *Lab Chip* **2009**, *9* (22), 3243. https://doi.org/10.1039/b911412m.

(9) Minghao, Y.; Kangkang, L.; Jiachen, Y.; Guanghui, W. Point-of-Care Immunoassay Centrifugal Microfluidics for Gastrin-17 Detection. In *2020 IEEE 5th Optoelectronics Global Conference (OGC)*; IEEE, 2020; pp 204–206. https://doi.org/10.1109/OGC50007.2020.9260468.

(10) Suárez, G.; Jin, Y.-H.; Auerswald, J.; Berchtold, S.; Knapp, H. F.; Diserens, J.-M.; Leterrier, Y.; Månson, J.-A. E.; Voirin, G. Lab-on-a-Chip for Multiplexed Biosensing of Residual Antibiotics in Milk. *Lab Chip* **2009**, *9* (11), 1625. https://doi.org/10.1039/b819688e.

(11) Walsh, C. L.; Babin, B. M.; Kasinskas, R. W.; Foster, J. A.; McGarry, M. J.; Forbes, N. S. A Multipurpose Microfluidic Device Designed to Mimic Microenvironment Gradients and Develop Targeted Cancer Therapeutics. *Lab Chip* **2009**, *9* (4), 545–554. https://doi.org/10.1039/B810571E.

(12) Zhang, Y.; Chen, X. The Mixing Performance of Passive Micromixers with Smart-Rhombic Units. *J Dispers Sci Technol* **2022**, *43* (3), 439–445. https://doi.org/10.1080/01932691.2020.1842759.

(13) Zeraatkar, M.; de Tullio, M. D.; Percoco, G. Fused Filament Fabrication (FFF) for Manufacturing of Microfluidic Micromixers: An Experimental Study on the Effect of Process Variables in Printed Microfluidic Micromixers. *Micromachines (Basel)* **2021**, *12* (8). https://doi.org/10.3390/mi12080858.

(14) Lee, C.-Y.; Chang, C.-L.; Wang, Y.-N.; Fu, L.-M. Microfluidic Mixing: A Review. *Int J Mol Sci* **2011**, *12* (5), 3263–3287. https://doi.org/10.3390/ijms12053263.

(15) Sudarsan, A. P.; Ugaz, V. M. Fluid Mixing in Planar Spiral Microchannels. *Lab Chip* **2006**, *6* (1), 74–82. https://doi.org/10.1039/b511524h.

(16) Ahmadi, V. E.; Butun, I.; Altay, R.; Bazaz, S. R.; Alijani, H.; Celik, S.; Warkiani, M. E.; Koşar, A. The Effects of Baffle Configuration and Number on Inertial Mixing in a Curved Serpentine Micromixer: Experimental and Numerical Study. *Chemical Engineering Research and Design* **2021**, *168*, 490–498. https://doi.org/10.1016/j.cherd.2021.02.028.

(17) Luong, T.-D.; Phan, V.-N.; Nguyen, N.-T. High-Throughput Micromixers Based on Acoustic Streaming Induced by Surface Acoustic Wave. *Microfluid Nanofluidics* **2011**, *10* (3), 619–625. https://doi.org/10.1007/s10404-010-0694-0.

(18) Jeon, H.; Massoudi, M.; Kim, J. Magneto-Hydrodynamics-Driven Mixing of a Reagent and a Phosphate-Buffered Solution: A Computational Study. *Appl Math Comput* **2017**, *298*, 261–271. https://doi.org/10.1016/j.amc.2016.11.026.

(19) Zhang, K.; Ren, Y.; Hou, L.; Feng, X.; Chen, X.; Jiang, H. An Efficient Micromixer Actuated by Induced-Charge Electroosmosis Using Asymmetrical Floating Electrodes. *Microfluid Nanofluidics* **2018**, *22* (11), 130. https://doi.org/10.1007/s10404-018-2153-2.

(20) Kunti, G.; Bhattacharya, A.; Chakraborty, S. Rapid Mixing with High-Throughput in a Semi-Active Semi-Passive Micromixer. *Electrophoresis* **2017**, *38* (9–10), 1310–1317. https://doi.org/10.1002/elps.201600393.

(21) Rahbarshahlan, S.; Ghaffarzadeh Bakhshayesh, A.; Rostamzadeh Khosroshahi, A.; Aligholami, M. Interface Study of the Fluids in Passive Micromixers by Altering the Geometry of Inlets. *Microsystem Technologies* **2021**, *27* (7), 2791–2802. https://doi.org/10.1007/s00542-020-05067-2.

(22) Mariotti, A.; Galletti, C.; Brunazzi, E.; Salvetti, M. v. Steady Flow Regimes and Mixing Performance in Arrow-Shaped Micro-Mixers. *Phys Rev Fluids* **2019**, *4* (3), 034201. https://doi.org/10.1103/PhysRevFluids.4.034201.

(23) Sudarsan, A. P.; Ugaz, V. M. Multivortex Micromixing. *Proceedings of the National Academy of Sciences* **2006**, *103* (19), 7228–7233. https://doi.org/10.1073/pnas.0507976103.

(24) Li, T.; Chen, X. Numerical Investigation of 3D Novel Chaotic Micromixers with Obstacles. *Int J Heat Mass Transf* **2017**, *115*, 278–282. https://doi.org/10.1016/j.ijheatmasstransfer.2017.07.067.

(25) Chen, X.; Zhao, Z. Numerical Investigation on Layout Optimization of Obstacles in a Three-Dimensional Passive Micromixer. *Anal Chim Acta* **2017**, *964*, 142–149. https://doi.org/10.1016/j.aca.2017.01.066.

(26) Kwak, T. J.; Nam, Y. G.; Najera, M. A.; Lee, S. W.; Strickler, J. R.; Chang, W.-J. Convex Grooves in Staggered Herringbone Mixer Improve Mixing Efficiency of Laminar Flow in Microchannel. *PLoS One* **2016**, *11* (11), e0166068. https://doi.org/10.1371/journal.pone.0166068.

(27) Hoffmann, M.; Schlüter, M.; Räbiger, N. Experimental Investigation of Liquid–Liquid Mixing in T-Shaped Micro-Mixers Using μ-LIF and μ-PIV. *Chem Eng Sci* **2006**, *61* (9), 2968–2976. https://doi.org/10.1016/j.ces.2005.11.029.

(28) Tsai, R. T.; Wu, C. Y. An Efficient Micromixer Based on Multidirectional Vortices Due to Baffles and Channel Curvature. *Biomicrofluidics* **2011**, *5* (1). https://doi.org/10.1063/1.3552992.

(29) Cetkin, E.; Miguel, A. F. Asymmetric Y-Shaped Micromixers with Spherical Mixing Chamber for Enhanced Mixing Efficiency and Reduced Flow Impedance. *Journal of Applied Fluid Mechanics* **2021**, *14* (5). https://doi.org/10.47176/jafm.14.05.32317.

(30) Abdelgawad, M.; Wu, C.; Chien, W. Y.; Geddie, W. R.; Jewett, M. A. S.; Sun, Y. A Fast and Simple Method to Fabricate Circular Microchannels in Polydimethylsiloxane (PDMS). *Lab Chip* **2011**, *11* (3), 545–551. https://doi.org/10.1039/c0lc00093k.

(31) Song, S.-H.; Lee, C.-K.; Kim, T.-J.; Shin, I.; Jun, S.-C.; Jung, H.-I. A Rapid and Simple Fabrication Method for 3-Dimensional Circular Microfluidic Channel Using Metal Wire Removal Process. *Microfluid Nanofluidics* **2010**, *9* (2–3), 533–540. https://doi.org/10.1007/s10404-010-0570-y.

(32) COMSOL Multiphysics 5.4, COMSOL Inc., 2018

(33) Web Plot Digitizer, https://apps.automeris.io/wpd/